

1           **Reassessing seasonal sea ice predictability of the Pacific-Arctic sector using**  
2   **a Markov model**

3           Yunhe Wang<sup>1,4</sup>, Xiaojun Yuan<sup>2</sup>, Haibo Bi<sup>1,3,4</sup>, Mitchell Bushuk<sup>5</sup>, Yu Liang<sup>1,6</sup>,  
4   Cuihua Li<sup>2</sup>, Haijun Huang<sup>1,3,4,6</sup>

5           <sup>1</sup> CAS Key Laboratory of Marine Geology and Environment, Institute of Oceanology,  
6   Chinese Academy of Sciences, Qingdao, China.

7           <sup>2</sup> Lamont-Doherty Earth Observatory of Columbia University, New York, USA.

8           <sup>3</sup> Laboratory for Marine Geology, Qingdao National Laboratory for Marine Science  
9   and Technology, Qingdao, China.

10          <sup>4</sup> Center for Ocean Mega-Science, Chinese Academy of Sciences, Qingdao, China.

11          <sup>5</sup> National Oceanic and Atmospheric Administration/Geophysical Fluid Dynamics  
12   Laboratory, Princeton, New Jersey, USA

13          <sup>6</sup> University of Chinese Academy of Sciences, Beijing, China

14          Corresponding author: Xiaojun Yuan ([xyuan@ldeo.columbia.edu](mailto:xyuan@ldeo.columbia.edu))

15 **Abstract**

16 In this study, a regional linear Markov model is developed to assess seasonal sea ice  
17 predictability in the Pacific-Arctic sector. Unlike an earlier pan-Arctic Markov model  
18 that was developed with one set of variables for all seasons, the regional model  
19 consists of four seasonal modules with different sets of predictor variables,  
20 accommodating seasonally-varying driving processes. A series of sensitivity tests are  
21 performed to evaluate the predictive skill in cross-validated experiments and to  
22 determine the best model configuration for each season. The prediction skill, as  
23 measured by the sea ice concentration (SIC) anomaly correlation coefficient (ACC)  
24 between predictions and observations, increased by 32% in the Bering Sea and 18% in  
25 the Sea of Okhotsk relative to the pan-Arctic model. The regional Markov model's  
26 skill is also superior to the skill of an anomaly persistence forecast. SIC trends  
27 significantly contribute to the model skill. However, the model retains skill for  
28 detrended sea ice extent predictions up to 7 month lead times in the Bering Sea and  
29 the Sea of Okhotsk. We find that subsurface ocean heat content (OHC) provides a  
30 crucial source of prediction skill in all seasons, especially in the cold season, and  
31 adding sea ice thickness (SIT) to the regional Markov model has a substantial  
32 contribution to the prediction skill in the warm season but a negative contribution in  
33 the cold season. The regional model can also capture the seasonal reemergence of  
34 predictability, which is missing in the pan-Arctic model.

## 35 **1 Introduction**

36 Sea ice acts as a major component of the Arctic climate system through  
37 modulating the radiative flux, heat, and momentum exchanges between the ocean and  
38 the atmosphere (Peterson et al., 2017; Porter et al., 2011; Smith et al., 2017). Sea ice  
39 also modulates sea surface salinity, which is one of the key drivers for thermohaline  
40 circulations (Sévellec et al., 2017). The rapid retreat of Arctic sea-ice extent in the  
41 past few decades has been considered a key indicator of climate change (Koenigk et  
42 al., 2016; Swart, 2017). The decreasing Arctic sea ice extent contributes to polar  
43 temperature amplification (Kim et al., 2016; Screen and Francis, 2016), an increase in  
44 wintertime snowfall over Siberia, northern Canada, and Alaska (Deser et al., 2010),  
45 polar stratospheric cooling (Screen et al., 2013; Wu et al., 2016), and potentially  
46 contributes to a weakening of the mid-latitude jet (Francis and Vavrus, 2012) and  
47 increased frequency of cold Northern Hemisphere midlatitude winter events (Cohen et  
48 al., 2020; Meleshko et al., 2018).

49 The rapid retreat of summer Arctic sea ice extent has also created more  
50 commercial opportunities in the newly opened Arctic waters. The Northwest Passage  
51 (through northern Canada) and the Northern Sea Route (north of Russia) could offer  
52 faster and less expensive shipping between the Pacific and Atlantic (Smith and  
53 Stephenson, 2013). Information on the Arctic marine accessibility and ice-free season  
54 duration in the marginal ice zone would enable planning of merchant shipping,  
55 conservation efforts, resource extraction, and fishing activities. The growing polar  
56 ecotourism industry could also benefit from shrinking sea-ice cover. Therefore,  
57 increased efforts have been devoted to developing Arctic sea-ice forecast systems in  
58 recent decades.

59 Substantial efforts have gone toward developing both statistical and dynamical sea  
60 ice prediction models. Dynamic models numerically solve equations that govern the  
61 sea ice physics using sea-ice, ocean, and/or atmospheric conditions to initialize the  
62 models for each season (Bushuk et al., 2019; Bushuk et al., 2020; Bushuk et al., 2021;  
63 Dai et al., 2020; Msadek et al., 2014). Numerous studies using fully coupled general

64 circulation models (GCMs) have quantified the seasonal prediction skill of pan-Arctic  
65 sea ice extent (SIE) and have found forecast skill for detrended pan-Arctic SIE at lead  
66 times of 1 to 6 months (Blanchard-Wrigglesworth et al., 2015; Day et al., 2014b;  
67 Guemas et al., 2016a; Peterson et al., 2015; Sigmond et al., 2013). Bushuk et al.  
68 (2017a) evaluated regional Arctic sea ice prediction skill in a Geophysical Fluid  
69 Dynamics Laboratory (GFDL) seasonal prediction system. They found skillful  
70 detrended regional SIE predictions, and found that skill varied strongly with both  
71 region and season.

72 On the other hand, statistical methods are also appealing for seasonal sea ice  
73 predictions (Petty et al., 2017). Statistical models capture relationships between sea  
74 ice and oceanic, atmospheric, or time-lagged sea ice predictor. Recently, statistical  
75 methods have been used to provide sea ice field predictions using numerous  
76 techniques such as linear Markov model (Chen and Yuan, 2004; Yuan et al., 2016),  
77 vector autoregressive model (Wang et al., 2019a; Wang et al., 2016), deep neural  
78 network (Andersson et al., 2021; Chi and Kim, 2017; Wang et al., 2017), Bayesian  
79 logistic regression (Horvath et al., 2020), and the combination of complex networks  
80 and Gaussian process regression model (Gregory et al., 2020). In some cases,  
81 statistical models provide better performance than dynamical models (Hamilton and  
82 Stroeve, 2016). For example, Yuan et al. (2016) showed that a linear Markov model  
83 has skillful sea ice concentration (SIC) predictions up to 9-month lead times in many  
84 regions of the Arctic and that this statistical model consistently captured more sea ice  
85 prediction skill than NOAA/NCEP Climate Forecast System (CFSv2) and the  
86 Canadian seasonal and interannual prediction system at the seasonal time scale. The  
87 Markov model prediction skill also exhibits strong regional and seasonal dependence.

88 Two common characteristics of sea ice predictability emerged from both dynamic  
89 (e.g. CFSv2 and GFDL climate models) and statistical models (e.g. linear Markov  
90 models, and linear regression models). First, low prediction skill occurs in the Pacific  
91 sector of the Arctic, particularly in the Bering Sea and the Sea of Okhotsk, compared  
92 with other Arctic regions (Bushuk et al., 2017a; Yuan et al., 2016). Many factors may

93 lead to this low predictability. Bushuk et al. (2017a) suggest that less persistent sea ice  
94 anomalies in the North Pacific sector possibly lead to less predictability in the region  
95 by the GFDL dynamical model. The Markov model of Yuan et al. (2016) was built in  
96 multivariate empirical orthogonal functions (MEOF) space in the pan-Arctic and the  
97 leading modes are dominated by the large long-term trend and strong climate  
98 variability in the Atlantic sector (Figure 1). So the signal of sea ice variability in the  
99 Pacific sector could be under-represented in the model. Therefore, it is necessary to  
100 evaluate the sea ice predictability in the Pacific sector with a new regional model.

101 Second, many studies have shown evidence for an Arctic sea ice spring  
102 predictability barrier that causes forecasts initialized prior to May to be less skillful  
103 and imposes a relatively sharp limit on regional summer sea ice prediction skill  
104 (Bushuk et al., 2017a; Day et al., 2014b; Yuan et al., 2016). Spring sea ice variability  
105 is complicated by surface melt ponds. The sea ice driven processes in spring could be  
106 different from those in other seasons. The spring barrier may result from a sharp  
107 increase in predictability at melt onset, when sea-ice-albedo feedback acts to enhance  
108 and persist the preexisting export-generated mass anomaly (Bushuk et al., 2020). In  
109 addition, summer initialization months have little sea ice coverage and have little  
110 intrinsic memory of sea ice and, therefore, require another source of memory to  
111 provide winter SIE prediction skill.

112 Actually, re-emergence mechanisms can provide sources of sea ice predictability  
113 on time scales from a few months to 1 year (Blanchard-Wrigglesworth et al., 2011).  
114 The re-emergence mechanism mainly relies on the persistence of some sea-ice related  
115 variables such as sea ice thickness (SIT) and ocean temperature. Previous studies have  
116 shown that summer sea surface temperature (SST) anomalies can provide a significant  
117 source of SIE predictability in the ice growth season (Blanchard-Wrigglesworth et al.,  
118 2011; Bushuk and Giannakis, 2017; Cheng et al., 2016; Dai et al., 2020). Initializing  
119 the upper ocean heat content (OHC) in a seasonal prediction system can also yield  
120 remarkable regional skill for winter sea ice (Bushuk et al., 2017a). Moreover,  
121 assimilating SIT data can slightly improve the SIC forecast and particularly benefit  
122 the sea ice prediction in summer, which is attributed to the long-lived SIT anomalies  
123 and their impact on summer sea ice (Blockley and Peterson, 2018; Bushuk et al.,

124 2017b; Guemas et al., 2016b; Xie et al., 2016). Because sea ice is closely coupled  
125 with the atmosphere and the ocean, the sea ice predictability is provided by the  
126 intrinsic memory of sea ice and its related variables, and accurate initial conditions are  
127 of importance for sea ice predictions (Blanchard-Wrigglesworth et al., 2011; Guemas  
128 et al., 2016b). Current climate models used for sea ice predictions are usually  
129 initialized using various atmospheric and oceanic variables, such as SIC, SIT, OHC,  
130 SST, surface air temperature (SAT), or other data from existing reanalysis (Bushuk et  
131 al., 2017a; Dai et al., 2020; Kimmritz et al., 2019; Yuan et al., 2016).

132 In this study, we develop a regional linear Markov model for the seasonal  
133 prediction of SIC in the Pacific sector with a focus on understanding unique sea ice  
134 driving processes in different seasons. We follow the framework of the pan-Arctic  
135 linear Markov model (Yuan et al., 2016). Unlike the pan-Arctic model that was  
136 developed with one set of variables (SIC, SAT, SST) for all seasons and the entire  
137 Arctic region, the regional model consists of four modules with seasonal dependent  
138 variables, which isolate the dominant processes for each targeted season. Regional  
139 relevant predictors are evaluated. New variables, including surface net radiative flux,  
140 turbulent heat flux, and pressure and wind fields, as well as SIT and OHC, are  
141 introduced to the model experiments. Sea ice predictability is assessed at grid points  
142 and over all seasons, and subsequently compared with the pan-Arctic model and other  
143 dynamic models.

## 144 **2 Data and methodology**

### 145 **2.1 Data**

146 Building on the extensive literature studying the predictability and variability of  
147 sea ice (Bushuk and Giannakis, 2017; Bushuk et al., 2020; Guemas et al., 2016a;  
148 Horvath et al., 2021; Lenetsky et al., 2021; Yuan et al., 2016), we firstly chose many  
149 kinds of oceanic and atmospheric variables and examined their correlations with SIC.  
150 The results show that SIC is highly related to OHC in the upper 300 m, SIT, SST,  
151 SAT, surface net radiative flux, surface net turbulent heat flux, geopotential height  
152 and wind vector at different levels including 850 to 200 hPa. Due to the barotropic

153 nature of the polar troposphere (Chen, 2005; Ting, 1994) and the low correlation  
154 between sea level pressure and SIC, we chose geopotential height and wind vector at  
155 850 hPa to define the low-level atmospheric circulation, whose interaction with sea  
156 ice is stronger relative to that in higher levels. Therefore, we choose to define the  
157 atmosphere-ice-ocean coupled Arctic climate system with 9 variables: SIC, OHC in  
158 the upper 300 m, SIT, SST, SAT, surface net radiative flux, surface net turbulent heat  
159 flux, 850 hPa geopotential height, and 850 hPa wind vector.

160 Monthly SICs in  $25 \text{ km} \times 25 \text{ km}$  grids are obtained from the National Snow and  
161 Ice Data Center (NSIDC) from 1979 to 2020 (Comiso, 2017). The dataset is generated  
162 from brightness temperatures derived from Nimbus-7 Scanning Multichannel  
163 Microwave Radiometer (SMMR), Defense Meteorological Satellite Program (DMSP)  
164 -F8, -F11, and -F13 Special Sensor Microwave/Imager (SSM/I), and DMSP-F17  
165 Special Sensor Microwave Imager/Sounder (SSMIS) using the bootstrap algorithm.  
166 Monthly SITs are from the Pan-Arctic Ice-Ocean and Assimilating System (PIOMAS)  
167 model data. PIOMAS is a sea ice-ocean reanalysis product that compares reasonably  
168 well to available satellite, aircraft, and in situ SIT measurements (Schweiger et al.,  
169 2011). The system applies a 12-category SIT and enthalpy distribution (Zhang and  
170 Rothrock, 2003) and is driven by NCEP/NCAR reanalysis atmospheric forcing  
171 including 10-m surface winds and 2-m SAT.

172 All atmospheric variables and SST with a spatial resolution of  $1^\circ \times 1^\circ$  are from the  
173 latest European Centre for Medium-Range Weather Forecasts (ECMWF) reanalysis  
174 product ERA5 (Hersbach et al., 2020) and are applied to represent the conditions of  
175 the atmosphere and ocean. ERA5 is produced using the version of ECMWF's  
176 Integrated Forecast System (IFS), CY41R2, based on a hybrid incremental 4D-Var  
177 system, with 137 hybrid sigma/pressure (model) levels in the vertical direction, with  
178 the top-level at 0.01 hPa. The OHC used here is global ocean and sea-ice reanalysis  
179 (ORAS5: Ocean Reanalysis System 5) monthly mean data and is developed by the  
180 European Centre for Medium-Range Weather Forecasts (ECMWF) OCEAN5 ocean  
181 analysis-reanalysis system (Zuo et al., 2019). ORAS5 includes five ensemble

182 members and covers the period from 1979 onwards. It is regarded as a global eddy-  
183 permitting ocean ensemble reanalysis product. Both the forcing fields and  
184 observational datasets are updated in ORAS5.

## 185 **2.2 The model**

186 The idea of using a Markov model for climate prediction is to build multivariate  
187 models, aiming to capture the co-variability in the atmosphere-ocean-sea ice coupled  
188 system instead of linearly regressing on individual predictors. Yuan et al. (2016)  
189 applied this statistical approach to predict SIC in the Arctic at a seasonal timescale  
190 and showed that the Lamont statistical model outperformed the NOAA CFSv2  
191 operational model and the Canadian Seasonal to Interannual Prediction System in sea  
192 ice prediction. They used MEOF as the building blocks of the model to filter out  
193 incoherent small-scale features that are basically unpredictable. Similar Markov  
194 models were also developed to study ENSO predictability (Cañizares et al., 2001; Xue  
195 et al., 2000) and for East Asian monsoon forecasts (Wu et al., 2013). The success of  
196 the Markov model is attributed to the dominance of several distinct modes in the  
197 coupled atmosphere-ocean-sea ice system and to the model's ability to pick up these  
198 modes.

199 Here we focus on the atmosphere-ocean-sea ice interactive processes that are  
200 unique to the Pacific sector and develop a regional linear Markov model for the  
201 seasonal prediction of SIC. The model consists of four modules with seasonally  
202 dependent variables. The model domain extends from 40°N to 84°N in latitude and  
203 from 120°E to 240°E in longitude (Figure 1). To reduce model dimensions, we  
204 remove land grid cells, mostly open water grid cells and mostly 100% ice cover grid  
205 cells from the sea ice field. The mostly open water cells are defined by the grids  
206 where  $SIC \geq 15\%$  only occurred less than 4% of the total all-season time series (492  
207 months), and mostly ice covered cells are defined by the grids where  $SIC \geq 95\%$  for  
208 more than 96% of total time series. SIC at the rest grid cells ranges from 0 to 100%.



209 Our model is constructed in the MEOF space. The base functions of the model's  
 210 spatial dependence consist of the eigenvectors from the MEOF, while the temporal  
 211 evolution of the model is a Markov process with its transition functions determined  
 212 from the corresponding principal components (PCs). We use only several leading  
 213 MEOF modes, which greatly reduce model space and filter out unpredictable small-  
 214 scale features. This method of reducing model dimension has been successfully used  
 215 in earlier Antarctic and Arctic sea ice predictability studies (Chen and Yuan, 2004;  
 216 Yuan et al., 2016).

217 We preselect SIC, OHC, SIT, SST, SAT, surface net radiative flux, surface net  
 218 turbulent heat flux, and geopotential height and winds at 850 hPa to represent  
 219 different sea ice-driving processes in the Pacific sector. We create anomaly time  
 220 series for all variables from 1979 to 2020 by subtracting climatologies of the same  
 221 period from monthly mean data. A normalization is applied to the time series at each  
 222 grid point for all variables. To emphasize sea ice variability in the model construction,  
 223 we weight SIC by 2 and other variables by 1, although the final model skill is not very  
 224 sensitive to this choice of weight. The weighted variables are stacked up into a single  
 225 matrix  $\mathbf{V}(n, m)$ , where  $n$  is the number of grid points of all fields and  $m$  is the length  
 226 of the time series. We then decompose  $\mathbf{V}$  into eigenvectors (spatial patterns)  $\mathbf{E}$  and  
 227 their corresponding PCs (time series)  $\mathbf{P}$ :

$$228 \quad \mathbf{V} = \mathbf{E}\mathbf{P}^T, \quad (1)$$

229 where the columns of  $\mathbf{E}$  are orthogonal and the columns of  $\mathbf{P}$  are orthonormal; the  
 230 superscript T denotes matrix transpose. It greatly reduces the model space by  
 231 truncating (1) to the several leading modes. The Markov model is computed using the  
 232 single-step correlation matrix, that is, a transition matrix  $\mathbf{A}$  that satisfies the following  
 233 linear relation:

$$234 \quad \mathbf{P}_{i+1} = \mathbf{A}\mathbf{P}_i + e_i, \quad (2)$$

235 where  $i$  denotes the  $i$ th month and  $e_i$  is the error in the model fit. Transition  $\mathbf{A}$  is  
 236 calculated by multiplying (2) with  $\mathbf{P}_i^T$

237 
$$\mathbf{P}_{i+1}\mathbf{P}_i^T = \mathbf{A}\mathbf{P}_i\mathbf{P}_i^T + e_i\mathbf{P}_i^T, \quad (3)$$

238 For the best model fit,  $e_i$  and  $\mathbf{P}_i^T$  should have no correlation. Thus

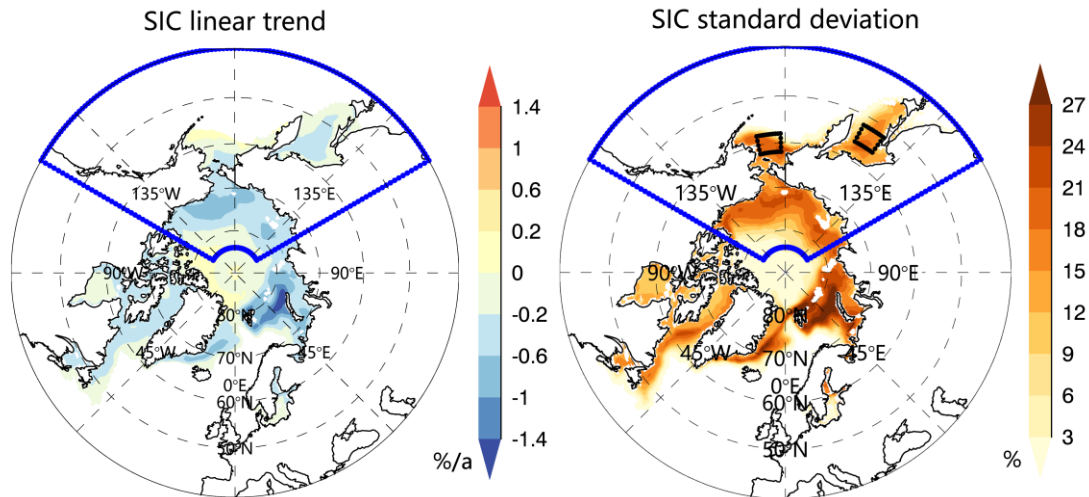
239 
$$\mathbf{A} = (\mathbf{P}_{i+1}\mathbf{P}_i^T)(\mathbf{P}_i\mathbf{P}_i^T)^{-1}. \quad (4)$$

240  $\mathbf{A}$  is constructed to be seasonally-dependent because of the strong seasonality of SIC  
 241 and related variables. Thus (4) is applied to 12 subsets of PCs to obtain different  
 242 transition matrices for each of the 12 calendar months.

243 After the Markov model is formulated, the SIC prediction can be generated  
 244 through the following eight steps: 1) to examine which variables have the highest  
 245 prediction potential in the Pacific sector, we create 10 climate variable combinations  
 246 representing different driving processes. 2) The PCs corresponding to each initial  
 247 multivariate space are calculated by the MEOF equation (1). 3) Transition matrices,  
 248  $\mathbf{A}$ , for each calendar month are calculated by equation (4). 4) The predictions of the  
 249 PCs are made by truncating to the first several modes and applying the appropriate  
 250 transition matrices at different lead times. “Lead time” refers to the number of months  
 251 prior to the target month that the forecast was initialized. For example, lead-1  
 252 prediction of January SIE is based on December data. 5) The predicted PCs are  
 253 combined with the respective eigenvectors to produce a spatially-resolved SIC  
 254 anomaly prediction for each variable combination. 6) We evaluate the prediction skill  
 255 measured by the SIC anomaly correlation coefficient (ACC), percentage of grid points  
 256 with significant ACC (PGS), and root mean square error (RMSE) using cross-  
 257 validated model experiments to identify the superior model for each season. 7) The  
 258 complete SIC anomaly prediction can then be generated by combining predicted PCs  
 259 by the corresponding optimal model in each season with eigenvectors. We  
 260 differentiate the seasons as follows: winter (December through February), spring  
 261 (March through May), summer (June through August), and autumn (September  
 262 through November). 8) The predicted SIC anomalies are divided by weight value 2,  
 263 multiplied by standard deviation, and added the climatology to generate the complete  
 264 prediction field.

265 To determine model variables and the number of modes to be used in the model,  
266 we evaluate the prediction skill at all grid points and all seasons in a cross-validated  
267 fashion for the period 1980-2020, by calculating the ACC and RMSE between  
268 predictions and observations. Notably, the dramatic declining trend in SIC prohibits  
269 us to use the first half of the time series for training the model and the second half of  
270 the time series to validate the model since the climate system mean state has changed  
271 dramatically over the last four decades. Another cross-validation scheme (Barnston  
272 and Ropelewski, 1992) is jackknifing, where one case is withheld from the regression  
273 development in the Markov model as an independent sample for testing. Thus, we  
274 built a Markov model for each month with a 1-yr moving window of data removal,  
275 and then used this window of predictions to evaluate the model performance. Here,  
276 we subtract one-year data from PCs and recalculate the transition matrix in equation  
277 (4); then twelve-month predictions are generated for that year. This procedure is  
278 repeated for each year of the time series. Such a cross-validated experimental design  
279 reduces artificial skill without compromising the length of the time series.

280 The long-term trend is an essential part of the Arctic sea ice variability. A  
281 substantial declining trend exists in Arctic SIC, particularly in the Barents Sea, the  
282 Kara Sea, the Beaufort Sea, and the Chukchi Sea (Figure 1). However, outside of the  
283 Arctic Basin, the long-term trends are relatively weak in the Pacific sector. As the  
284 trends are parts of the total variability, we retain the SIC trends in anomalies while  
285 building the model and then conduct a post prediction evaluation of the impact of  
286 trends on the model skill.



287

288 **Figure 1.** Arctic SIC trends (left) and standard deviation (right) computed using  
 289 SIC anomalies over all 12 months of the period 1979-2020. The Pacific-Arctic model  
 290 domain is enclosed by blue lines, which covers 40° - 84°N and 120° - 240°E. Two  
 291 focused areas marked in black boxes in the Bering Sea (between 58° - 62°N and 182° -  
 292 192°E) and the Sea of Okhotsk (between 52° - 56°N and 144° - 152°E) have large  
 293 standard deviations and are selected to evaluate the ACC skill improvement in the  
 294 regional model compared with the pan-Arctic Markov model developed by Yuan et  
 295 al. (2016).

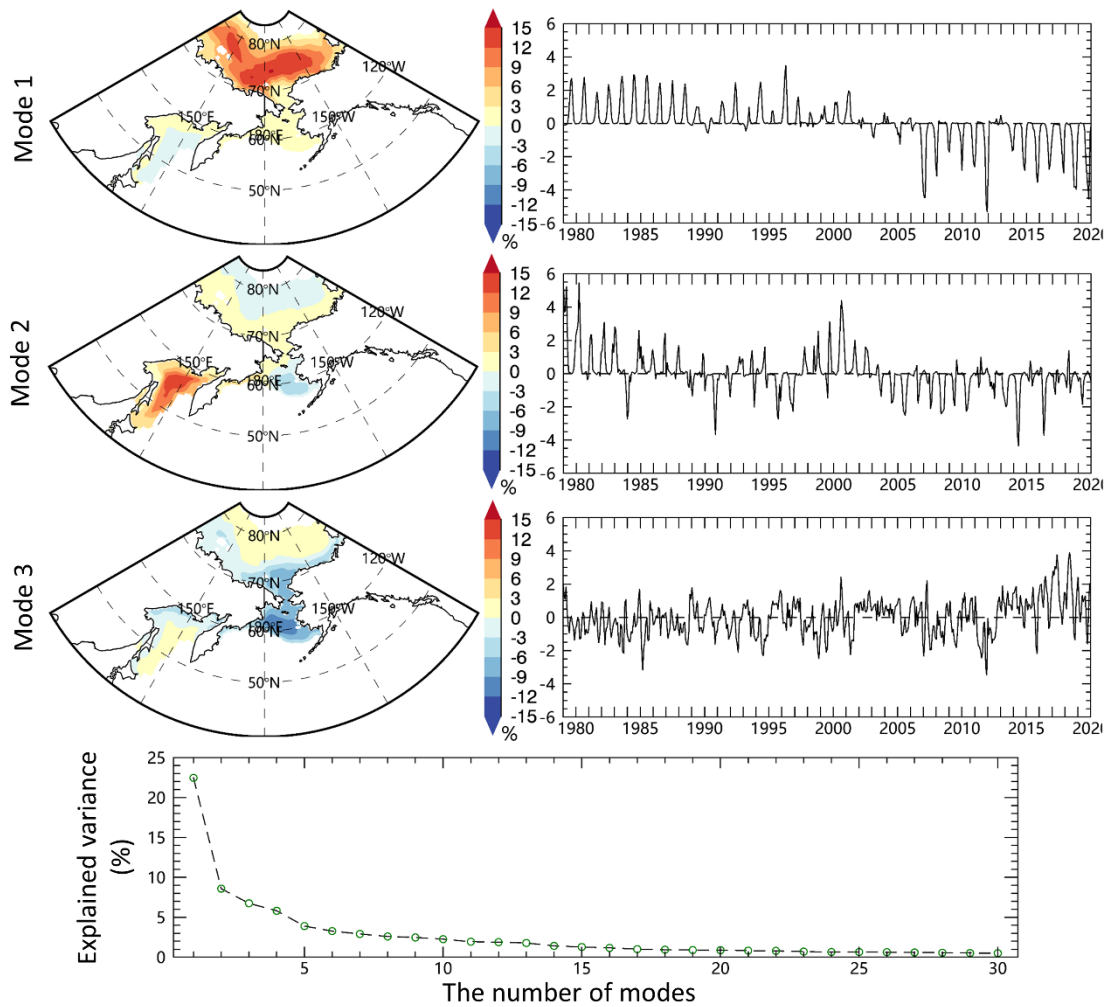
### 296 3 Model construction and assessments

#### 297 3.1 EOF analysis of Pacific SIC

298 Before constructing the model, we first examine whether the EOF analysis can  
 299 isolate the regional and seasonal SIC variability in the Pacific-Arctic sector. Figure 2  
 300 shows the eigenvectors of the three leading EOF modes of SIC. The first mode of SIC  
 301 variability, accounting for 23% of the total variance, mainly shows a positive pattern  
 302 within the Arctic Basin from 1979 to 2002 and a negative pattern after 2003 with a  
 303 record low in 2007 and 2012, representing the decreasing trend in summer and early  
 304 fall SIC. The declining trend is heavily loaded inside the Arctic Basin from the East  
 305 Siberian Sea to the Beaufort Sea. The second SIC mode (9% of total variance)  
 306 primarily captures out-of-phase SIC anomalies in the Bering Sea and the Sea of

307 Okhotsk and is associated with the Aleutian-Icelandic low seesaw, representing SIC  
308 variability in cold seasons (Frankignoul et al., 2014). This pattern suggests  
309 consistently positive SIC anomalies in the Bering Sea and negative anomalies in the  
310 Sea of Okhotsk after 2004. The SIC variability in the central sector (approximately  
311 60°-70°N) stands out in the third EOF mode (7% of the total variance), which is a  
312 commonly observed feature in the region during spring and autumn. This finding  
313 shows that the EOF (MEOF) analysis can well isolate the regional and seasonal SIC  
314 variability including the trend in the Pacific-Arctic sector.

315 We further divided the SIC time series into four seasons and conducted EOF  
316 analysis respectively. The results show that fewer modes can explain the dominant  
317 SIC variance in autumn and summer benefiting from the large SIC variability and  
318 trend (Figure S1). For example, the leading 10 modes can explain 70% of the SIC  
319 total variance in autumn and summer, while about 25 modes are needed for explaining  
320 the same amount of variance in cold seasons. It turns out that the several leading  
321 modes can explain the dominant SIC variability. This is an important premise to  
322 reduce the model dimension and, more importantly, to filter out incoherent small-  
323 scale features that are likely unpredictable. In addition, it is necessary to build the sea  
324 ice prediction model for individual seasons because of the differences in seasonal  
325 patterns of variability and the different number of leading modes required to capture  
326 predictable variability.



327

328 **Figure 2.** The eigenvectors and PCs of the three leading EOF modes of SIC in the  
 329 Pacific-Arctic sector for the period 1979-2020. The bottom panel shows the explained  
 330 variance as a function of the number of leading modes of SIC.

### 331 3.2 Construct an optimal model for each season

332 A practical issue in building a Markov model in MEOF spaces is which  
 333 combination of variables and number of leading modes to retain in the model. Using  
 334 too few modes may miss some predictable signals, and too many may result in  
 335 overfitting and contaminate the model with incoherent small-scale features. To  
 336 determine optimal predictor variables and reasonable mode truncations, we calculate  
 337 the prediction skill from a series of cross-validated model experiments, which used  
 338 different numbers of modes and different variables. Table 1 shows the detailed  
 339 variable-combinations. Models V2-V4, V6-V8, and V10-V11 are weighted toward

340 thermodynamic processes, whereas V9 and V12 represent integration of  
 341 thermodynamic and dynamic processes.

342 **Table 1.** Variable combinations in cross-validated experiments. V1 represents the  
 343 No. 1 variable-combination. ✓ represents the variable included in the corresponding  
 344 combination.

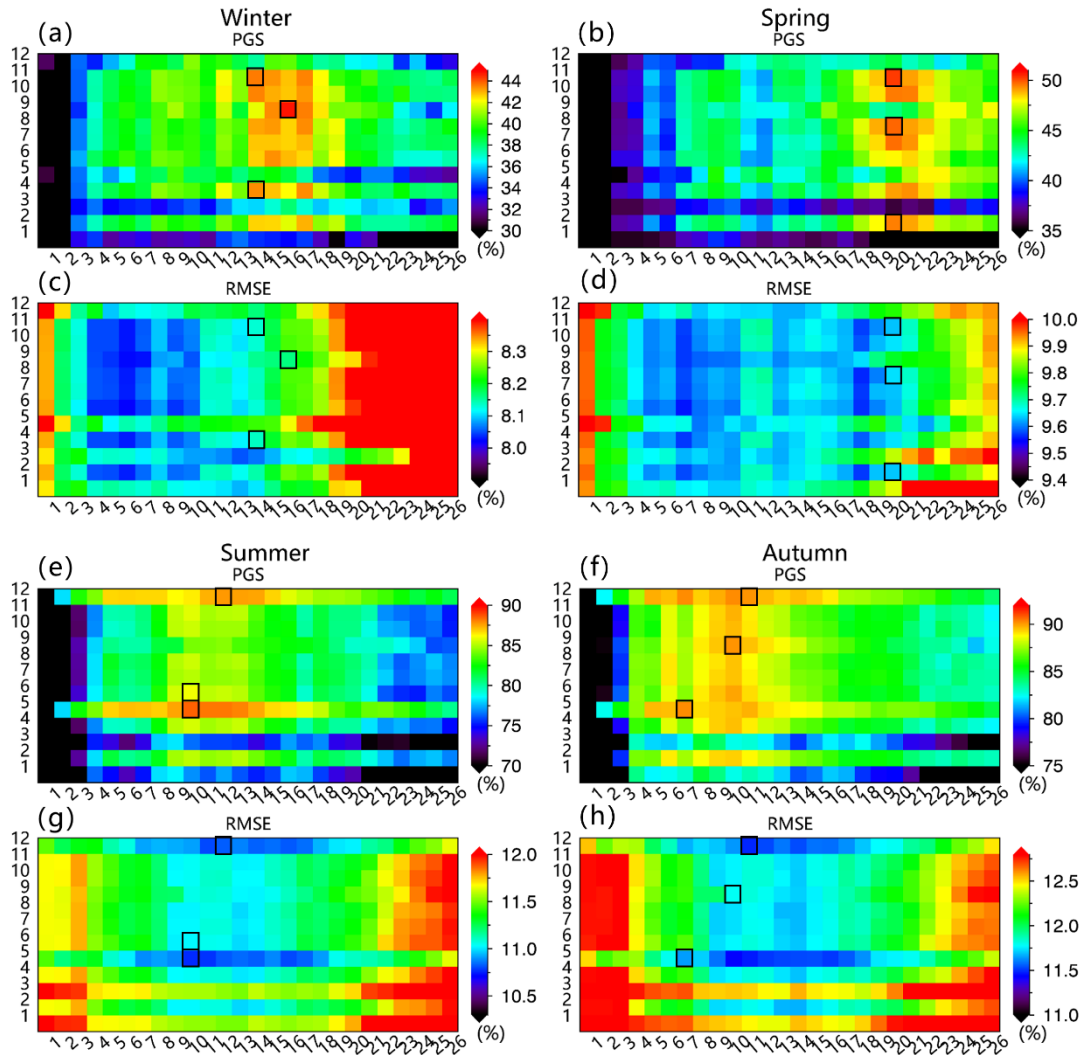
	V1	V2	V3	V4	V5	V6	V7	V8	V9	V10	V11	V12
SIC	✓	✓	✓	✓	✓	✓	✓	✓	✓	✓	✓	✓
OHC		✓		✓	✓	✓	✓	✓	✓	✓	✓	✓
SST			✓	✓						✓	✓	✓
SIT					✓							✓
SAT						✓						✓
Surface net turbulent heat flux								✓			✓	✓
Surface net radiative flux							✓			✓		✓
850hPa GPH, U, V									✓			✓

345 The cross-validation scheme is carried out for the time series to produce  
 346 predictions at 1- to 12-month lead. The PGS and mean RMSE for each lead time in  
 347 each season are calculated. To avoid missing predictable signals, we initially retain  
 348 large amounts of modes (up to 52) in the model and then narrow the range of mode  
 349 numbers to determine the best model configuration for each season. Figure S2  
 350 presents the PGS for each lead time for winter target months. It shows that the model  
 351 prediction skill in winter steeply decreases after 36 modes in most lead months.  
 352 Similarly, RMSE increases rapidly after 36 modes (Figure S3). This indicates that  
 353 including modes beyond mode 36 in winter, mainly representative of unpredictable  
 354 small-scale features, leads to the rapid decrease of predictive skill.

355 To select a model configuration that fits all lead times, we average the 12 panels  
 356 in Figures S2 and S3, respectively, and display them in the first column of Figure S4.  
 357 Similarly, predictive skills for other seasons are also examined. We further narrow the  
 358 modes' range to display the predictive skill according to Figure S4 so that we can  
 359 determine the optimal model more accurately (Figure 3). Generally, the model skills  
 360 are better in summer and autumn than in winter and spring, and more modes are

361 needed in the cold season to capture the predictable signal of SIC, which is likely due  
 362 to the weaker trends in these months. Models with high correlation also have smaller  
 363 RMSE but the RMSE differences between models are relatively small.

364



365

366 **Figure 3.** Mean PGS and mean RMSE between the observations and predictions  
 367 in four seasons. (a) Mean PGS is obtained by averaging all lead months for winter  
 368 predictions. The x-axis represents the number of MEOF modes, and the y-axis  
 369 represents the combination of the variables corresponding to Table 1. (b, e, and f) are  
 370 the same as (a) except for spring, summer, and autumn respectively. (c, d, g, and h)  
 371 are the same as (a, b, e, and f) except for RMSE.



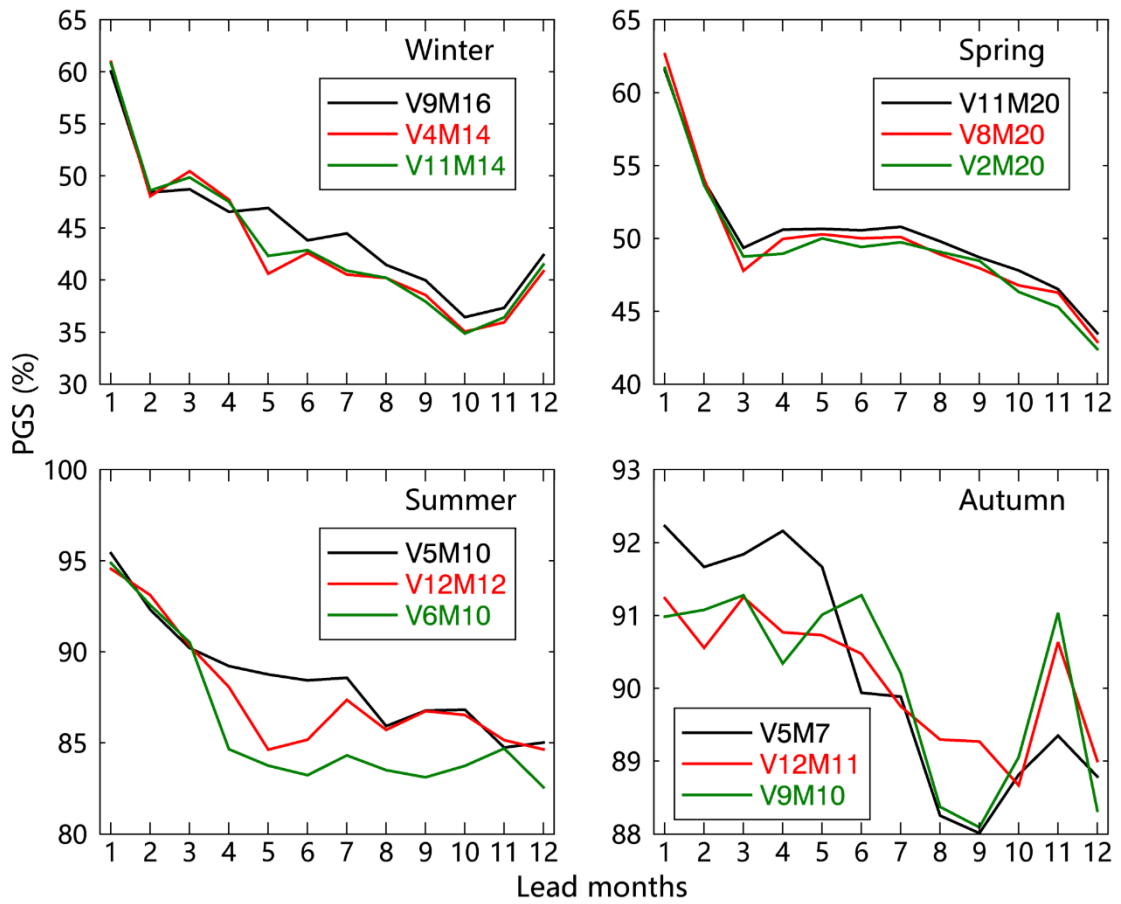
372 Based on the PGS and RMSE, we primarily chose three superior model  
373 configurations marked by black boxes in Figure 3 for each season respectively. To  
374 determine which model configuration produces the best prediction in each season, we  
375 spatially average the SIC prediction skill from these superior models with 1- to 12-  
376 month leads (Figures 4 and 5). Figure 4 shows the cross-validation skill measured by  
377 PGS. In general, the predictive skill in the warm season is higher than that in the cold  
378 season, although the RMSEs are also relatively large in the warm season (Figure 5).  
379 The model prediction skills based on those superior model configurations have similar  
380 variability and magnitude in winter and spring respectively, while large differences of  
381 that occur in the warm season, especially in autumn. It also shows that the model  
382 prediction skill steeply decreases at the 2-month lead in winter and at the 2- and 3-  
383 month lead in spring.

384 As a model construction principle, we choose the minimum number of variables  
385 and modes to achieve the same level of skill, avoiding possible overfitting. Based on  
386 the PGS and RMSE, we chose V9M16 as the best model in winter since it shows the  
387 highest PGS. Similarly, we chose V11M20 in spring and V5M10 in summer. In  
388 autumn, The model skill from V5 is obviously superior at 1-5 lead months, while V12  
389 dominates prediction skill beyond the 8-month lead. We decided to choose V5M7  
390 because it has a relatively higher mean skill and fewer variables and modes.

391 The contribution of different variables in ice prediction skill for each season is  
392 also assessed. OHC contributes more model prediction skill than SST in all seasons  
393 (Figure 3). The model built on the data matrix of SIC, OHC performs better in winter  
394 and spring, which indicates that the OHC provides a considerable source of memory  
395 for SIC prediction skill in the cold season and plays a key role in the evolution of sea  
396 ice conditions. The results are consistent with many previous studies (Bushuk et al.,  
397 2017a; Dai et al., 2020; Guemas et al., 2016b; Lenetsky et al., 2021). 850 hPa  
398 geopotential height and winds can still contribute additional prediction skill in winter  
399 since including OHC, geopotential height and winds slightly outperforms the case  
400 without geopotential height and winds (Figure 4). 850 hPa GPH and wind not only

401 affect the heat and moisture transport by atmospheric circulation anomaly but also  
402 drive sea-ice drift. For example, the dipole structure anomaly of the Arctic  
403 atmospheric circulation shows strong meridionality and plays a profound role in sea-  
404 ice export/import, and heat and moisture transport through the Pacific-Arctic sector  
405 (Wu et al., 2006).

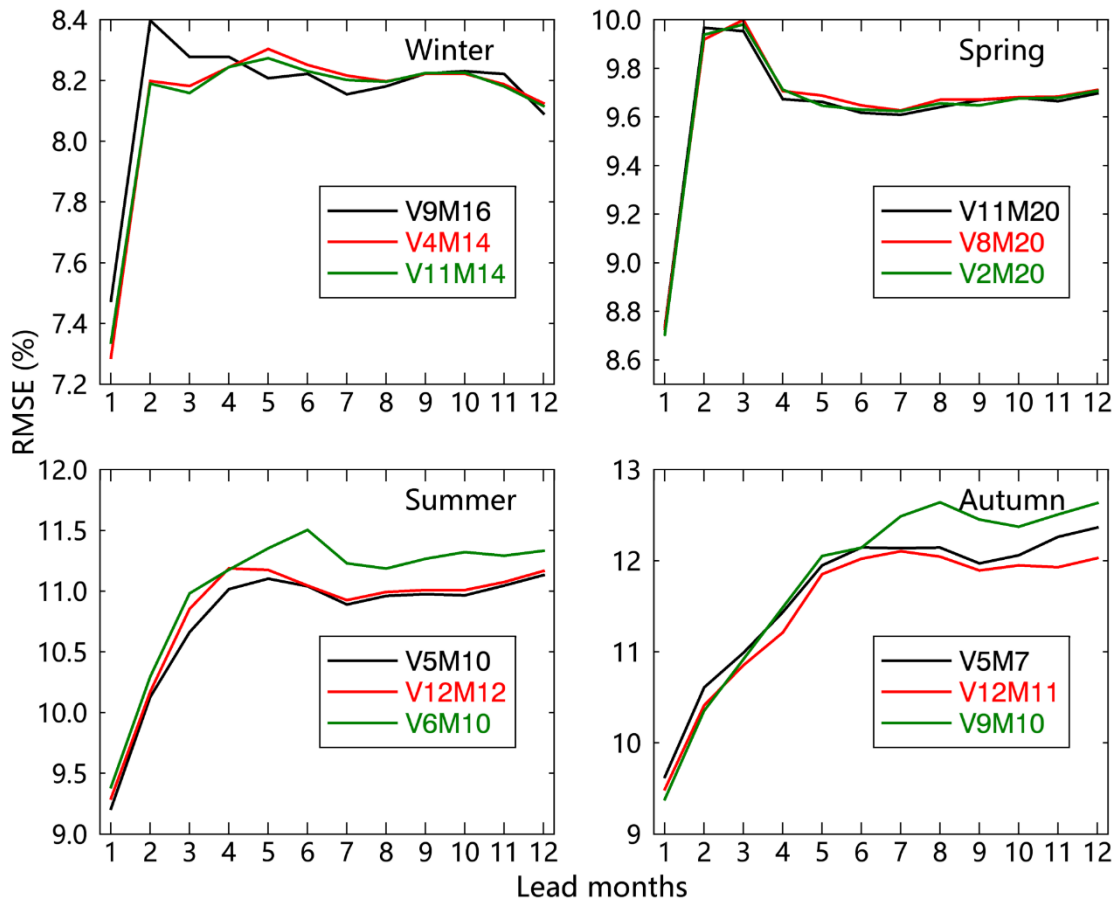
406 Similarly, SST and turbulent heat flux also contribute additional skill in spring  
407 although the contribution is minor (Figures 3 and 4). It is worth mentioning that the  
408 variable such as SST with minor additional contributions to the model does not mean  
409 that it is a minor contributor since the contributions from different variables to  
410 prediction skill partially overlap. In addition, adding SIT to the model has a  
411 substantial contribution to the prediction skill in the warm season, indicating that sea  
412 ice thickness is a key source of sea ice predictability within the Arctic Basin in the  
413 warm season especially in summer, which is consistent with previous studies  
414 (Blanchard-Wrigglesworth et al., 2011; Blockley and Peterson, 2018; Day et al.,  
415 2014a; Morioka et al., 2021; Tian et al., 2021; Yuan et al., 2016). However, SIT has a  
416 negative contribution to the prediction skill in the cold season (Figure 3). The  
417 contributions of SIT to the prediction skill in autumn are very sensitive to the number  
418 of lead months that the skill steeply decreases beyond a 5-month lead (Figure 4). In  
419 other words, the model didn't perform well in autumn prediction initialized in winter  
420 and spring. In addition, the surface net radiative flux also contributes to the model  
421 skill in the cold season (Figure 3). Early studies suggested that the surface longwave  
422 radiation plays an indispensable role in the polar climate system in the cold season  
423 when shortwave radiation is at its annual minimum (Huang et al., 2015; Kapsch et al.,  
424 2013; Lee et al., 2017; Liu and Key, 2014; Luo et al., 2017; Wang et al., 2019b).



425

426

**Figure 4.** PGS for the preliminary selection of superior models in each season.



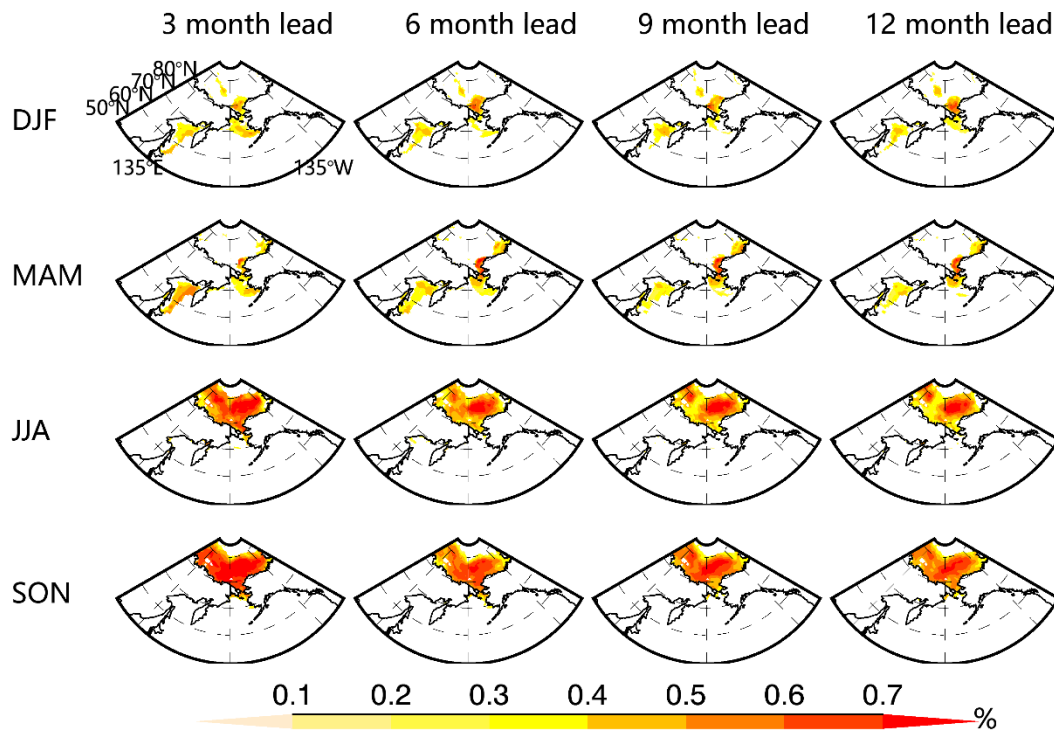
427

428 **Figure 5.** Same as Figure 4 but for RMSE.

429 **3.3 Assessment of model skill**

430 To test the forecast skill of the model, the SIC predictions were evaluated at each  
 431 grid cell and for all seasons using the ACC and RMSE between predicted and  
 432 observed anomalies, and the skill is presented at 3, 6, 9, and 12 lead months. In winter  
 433 (DJF), high forecast skill is concentrated in the Arctic marginal seas and peripheral  
 434 seas: the southern Chukchi Sea and Sea of Okhotsk (Figure 6). The skill is slightly  
 435 lower at a 12-month lead in the Sea of Okhotsk and a 9-month lead in the southern  
 436 Chukchi Sea. Overall, the winter skill is roughly 0.4 in the Sea of Okhotsk and 0.5 in  
 437 the southern Chukchi Sea at up to 12-month leads. The spring (MAM) prediction skill  
 438 shows a similar pattern as that in winter but with a 0.1 increase in the ACC skill. The  
 439 southern Chukchi Sea and Bering Strait have higher skills than the Bering Sea. For  
 440 summer (JJA) predictions, the prediction skill is concentrated in the Arctic basin since  
 441 sea ice totally melts in the Arctic peripheral seas. The 3-month lead prediction has the

442 highest skill ( $>0.6$ ) in most of the Arctic basin, while the lowest prediction skill ( $<0.5$ )  
 443 is found at a 12-month lead. The autumn (SON) prediction skill shows a similar  
 444 pattern as the summer skill but with higher correlations. In general, the model has  
 445 higher prediction skills for warm seasons, especially for autumn, than that for cold  
 446 seasons, while the lowest skill is in winter.



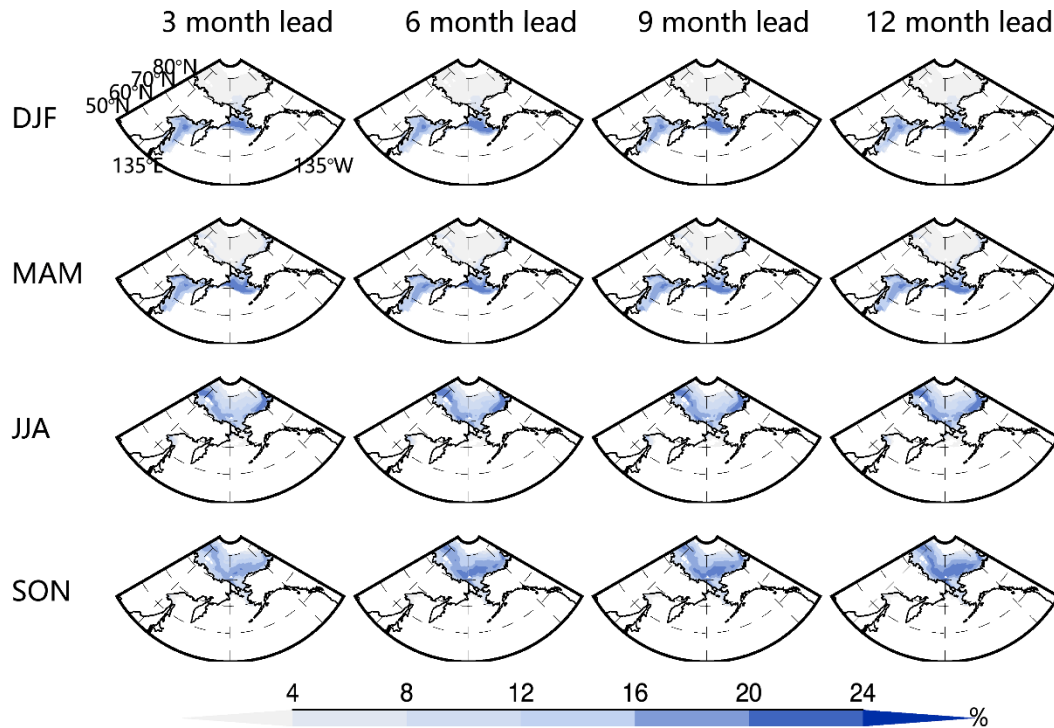
447

448 **Figure 6.** Cross-validated model skills measured by ACC between SIC  
 449 predictions and observation anomalies as a function of seasons and lead months. Only  
 450 the correlations that are significantly above the 95% confidence level based on a  
 451 Student's t test are included in the panels.

452 RMSEs are consistent with correlations: high correlations correspond to low  
 453 RMSEs, and vice versa, although minor inconsistencies occur in some seasons and  
 454 regions (Figure 7). The RMSE is large around the Arctic basin for the warm season  
 455 and in the peripheral sea for the cold season where SIC has large variability. In the  
 456 cold season, the RMSE is larger in the Bering Sea than that in the Sea of Okhotsk.  
 457 The magnitudes of RMSE remain at roughly the same level from 3- to 12-month lead  
 458 in most locations for all seasons. The marginal seas have larger RMSEs than the  
 459 central Arctic basin in both summer and autumn, while the error magnitudes in

460 autumn are slightly larger than those in summer but smaller than the SIC standard  
461 deviation across the Pacific sector (Figure 1).

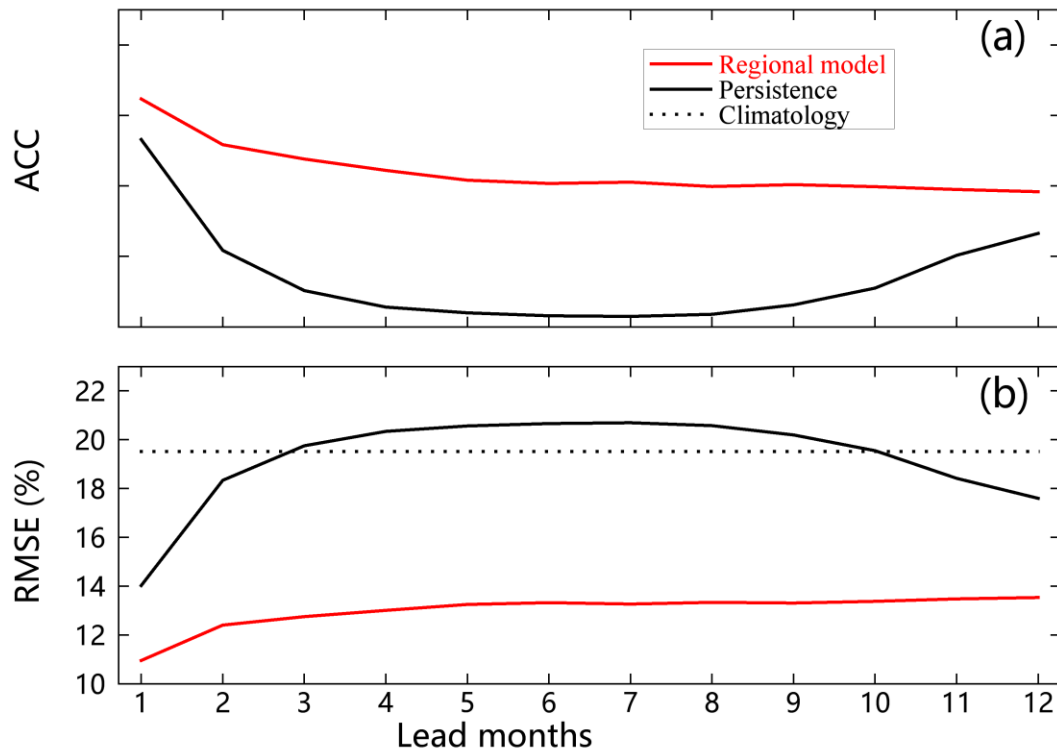
462



463

464 **Figure 7.** Same as Figure 6 except for RMSEs. The color bar is in a unit of  
465 percentage.

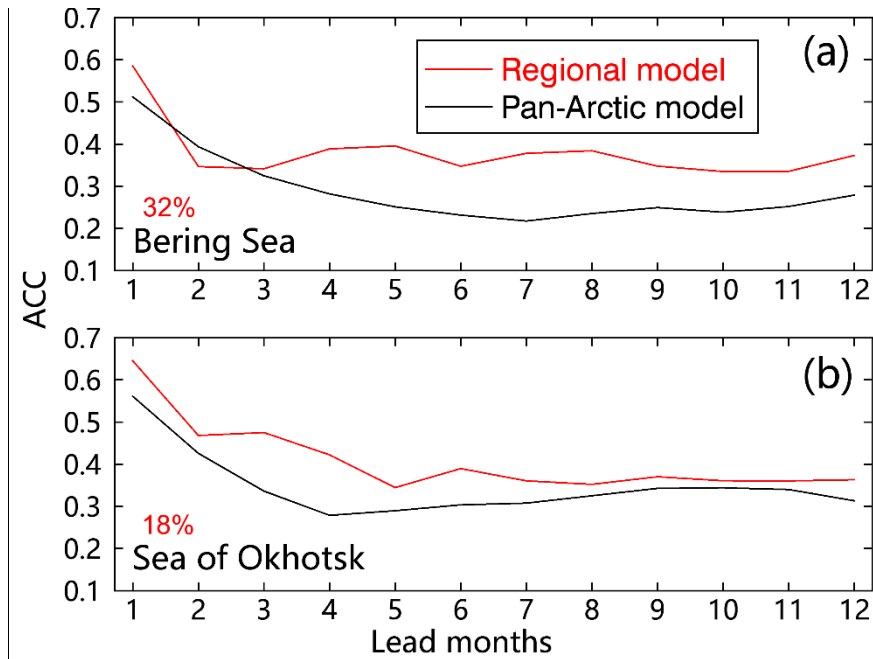
466 Also, the model performance is further evaluated against anomaly persistence and  
467 climatology. Averaged over the grid points in the model domain and over all seasons  
468 for the period of 1980-2020, the regional Markov model's mean correlation is  
469 manifestly higher, and the mean RMSE of the regional Markov model is much lower  
470 than the climatology and anomaly persistence for all the lead months, especially from  
471 2-month lead to 10-month lead (Figure 8). In addition, RMSE is not sensitive to the  
472 lead months, showing the superiority of the regional model. These results suggest that  
473 the regional Markov model can capture significantly more predictability beyond SIC  
474 anomaly persistence.



476

477 **Figure 8.** The prediction skill of the regional Markov model compared against  
 478 that of anomaly persistence and climatology averaged over the model domain as a  
 479 function of the number of month lead times.

480 To assess the regional model skill improvements from the pan-Arctic model  
 481 presented by Yuan et al. (2016), we calculated the ACC as a function of lead months  
 482 (Figure 9). Note that the ACC is calculated only in typical regions with large standard  
 483 deviations marked in Figure 1. The regional model evidently enhances the ACC skill  
 484 from the pan-Arctic model for the 4- to 12-month lead predictions in the Bering Sea  
 485 and the 1- to 7-month lead predictions in the Sea of Okhotsk. The mean ACC is also  
 486 increased by 32% in the Bering Sea and 18% in the Sea of Okhotsk. The prediction  
 487 skill of the regional Markov model within the Arctic basin also remains at the same  
 488 high level as that of the Pan-Arctic model (not shown), so significant skill  
 489 improvements occur in the peripheral sea of the Pacific sector.



490

491 **Figure 9.** Cross-validated model skills of the regional Markov model vs. the Pan-  
 492 Arctic Markov model. (a) The skills are measured by the ACC between predictions  
 493 and observations with trends from 1980 to 2020 as a function of lead months in the  
 494 Bering Sea. (b) is the same as (a) except for the Sea of Okhotsk. The red numbers in  
 495 the bottom left of each panel represent the mean regional model skill improvements  
 496 from the pan-Arctic model.

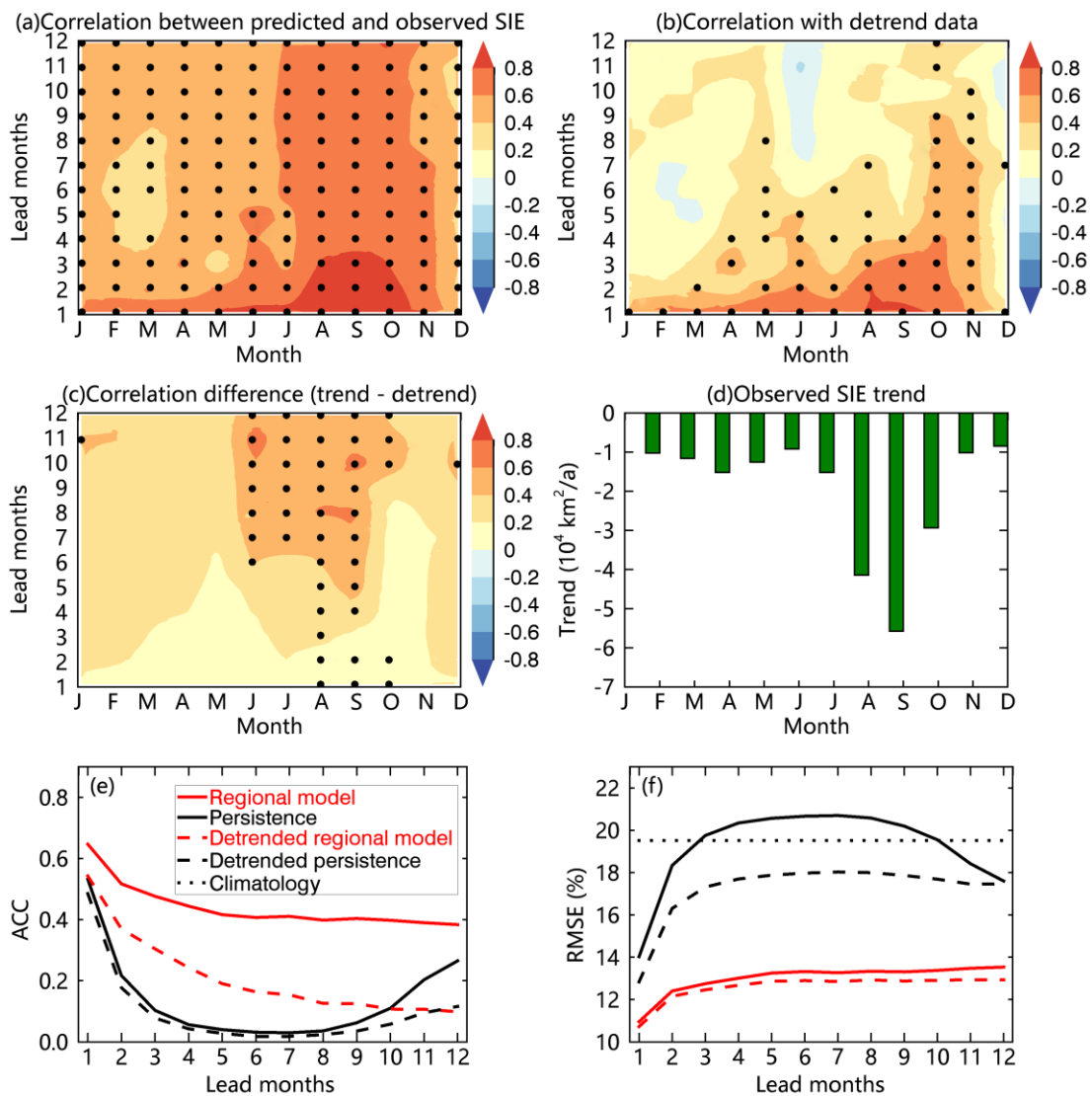
497 **4 Discussion**

498 **4.1 Contribution of linear trends to SIE prediction skill**

499 Sigmond et al. (2013) show that the linear trend in Arctic SIE dramatically  
 500 contributes to its forecast skill in the Canadian Seasonal to Interannual Prediction  
 501 System. Lindsay et al. (2008) show that their dynamic model prediction skill is much  
 502 lower when the trend is not included. They suggested that the trend accounts for 76%  
 503 of the variance of the pan-Arctic ice extent in September. The trend also contributes  
 504 to the pan-Arctic prediction in the linear Markov model (Yuan et al., 2016). In the  
 505 Arctic, SIE has declined at -0.35 million square kilometers per decade during 1979-  
 506 2020, which is significant at the 95% confidence level. The large SIC trend is mainly  
 507 in the Barents Sea and the Kara Sea, followed by the Chukchi Sea, while the mean  
 508 SIC trend in the Bering Sea and the Sea of Okhotsk is relatively weak (Figure 1). To



509 evaluate the contribution of long-term trends to the regional Markov model skill, we  
 510 conducted post-prediction analysis on linear trends' contribution to the predictions  
 511 skill of SIE in the Pacific-Arctic sector. We examine the time series of SIE in all  
 512 calendar and lead months calculated by summing the Pacific-Arctic areas that have at  
 513 least 15% SIC from observations and predictions. Monthly trends were removed from  
 514 the predictions and observations, respectively. Then, the model skill is compared  
 515 between the original SIE predictions and detrended SIE predictions.



516

517 **Figure 10.** (a) The SIE forecast skill of the regional Markov model as a function  
 518 of the calendar month and lead months. (b) The SIE forecast skill when monthly  
 519 trends are removed from the predictions and observations respectively. The black dots  
 520 in (a) and (b) represent the correlations that are significantly above the 95%

521 confidence level. (c) Difference between (a) and (b). The black dots in (c) indicate  
522 that the correlation differences are significant above the 95% confidence level. (d)  
523 Observed trends in SIE as a function of the calendar month. All monthly SIE trends  
524 are significantly above the 95% confidence level. (e, f) The prediction skill of the  
525 regional Markov model compared against that of anomaly persistence and  
526 climatology averaged over the model domain as a function of the number of month  
527 lead times.

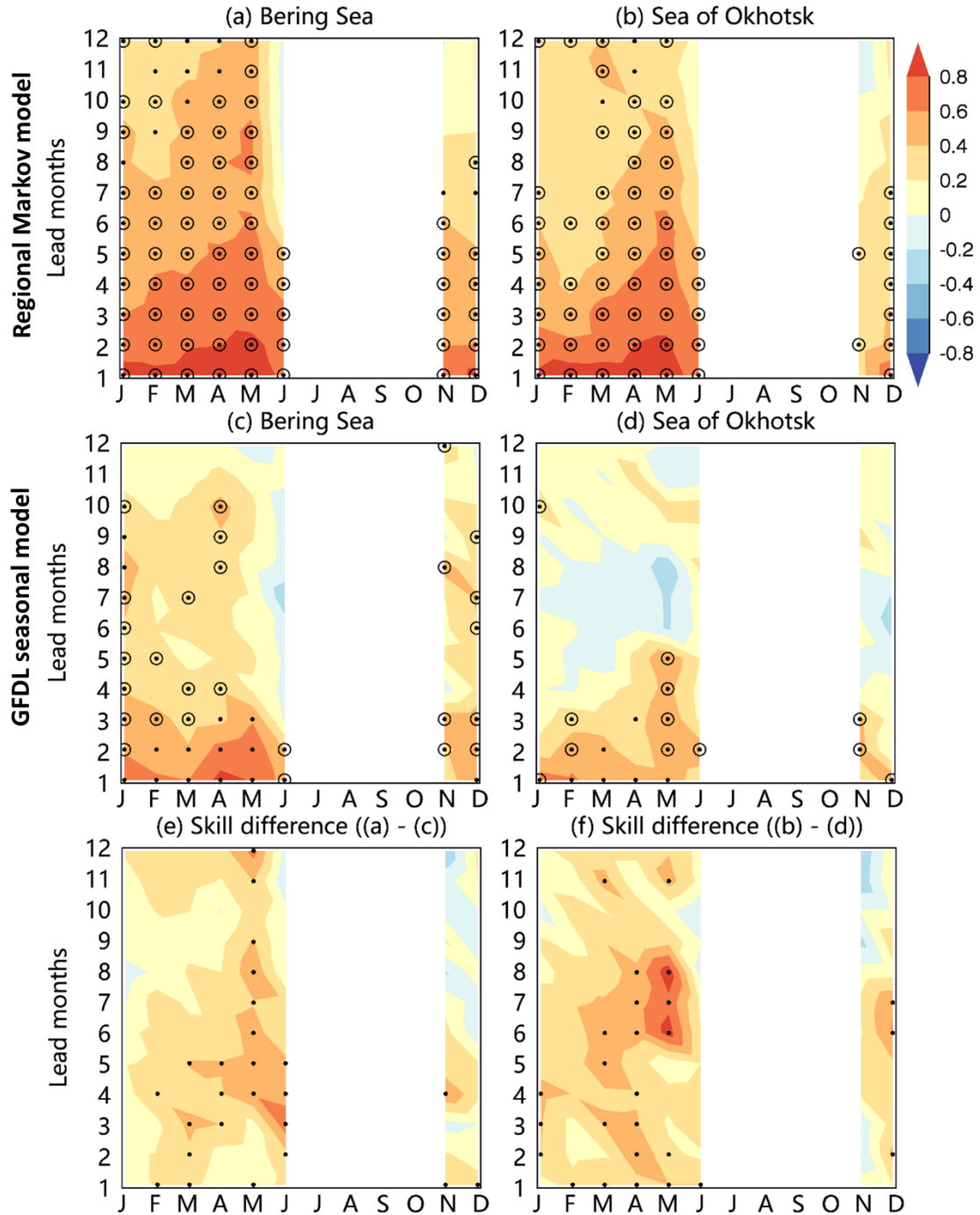
528 The model is skillful in predicting SIE from January to November at a 1-month  
529 lead (Figure 10a). The skill is particularly high for summer and autumn predictions,  
530 where ACC is higher than 0.6 from July through November even at a 12-month lead.  
531 The model skill is relatively low in May, especially at 4-8 lead months. This pattern is  
532 consistent with the seasonal variation of the model skill for SIC prediction presented  
533 in Figure 6. After monthly trends are removed from predictions and observations  
534 respectively, the model skill is significantly reduced for all seasons, especially for the  
535 warm season at 6-12 months lead (Figure 10b, c). This is consistent with the  
536 seasonality of the observed trend (Figure 10d), which also peaks in late summer and  
537 early fall.

538 Averaging the differences in Figure 10c over all lead times and predicted months,  
539 the trend removal results in a mean reduction of 0.31 from the SIE forecast skill; a  
540 53% reduction of the mean ACC. However, the model retains high prediction skill  
541 (0.61) from January to November at 1-2 lead months, representing a 19% reduction  
542 by the trend removal (Figure 10b), which shows the model's capability of capturing  
543 sea ice internal variability. In addition, the trend is relatively large in the Chukchi Sea  
544 and weak outside of the Arctic Ocean. The model only reduces 13% of the mean ACC  
545 from January to November at 1-2 lead months after the trend removal for the area  
546 outside of the Arctic Ocean. Although linear trends contribute significantly to the  
547 model skill, the regional Markov model's mean correlation is manifestly higher, and  
548 the mean RMSE of the regional Markov model is much lower than the climatology

549 and anomaly persistence for all the lead months when the sea ice trend is removed  
550 (Figure 10e, f).

## 551 **4.2 Comparison with the GFDL model**

552 Yuan et al. (2016) showed that the pan-Arctic Markov model consistently  
553 outperforms the NOAA/NCEP Climate Forecast System (CFSv2) and the Canadian  
554 seasonal and interannual prediction system for sea ice seasonal predictions. Here the  
555 regional Markov model is compared with the Geophysical Fluid Dynamics  
556 Laboratory Forecast-oriented Low Ocean Resolution (GFDL-FLOR) seasonal  
557 prediction system (Bushuk et al., 2017a) in detrended SIE forecasts. The hindcast  
558 model skills measured by the ACC for detrended SIE are high from both the regional  
559 Markov model and GFDL model during January to June at a 1- to 3-month lead in the  
560 Pacific sector (Figure 11). The regional Markov model skill is statistically significant  
561 at lead times ranging from 1 to 6 months for target months of January-June in both the  
562 Bering Sea and the Sea of Okhotsk. Below we highlight some key differences  
563 between these two models in the Bering Sea and the Sea of Okhotsk.



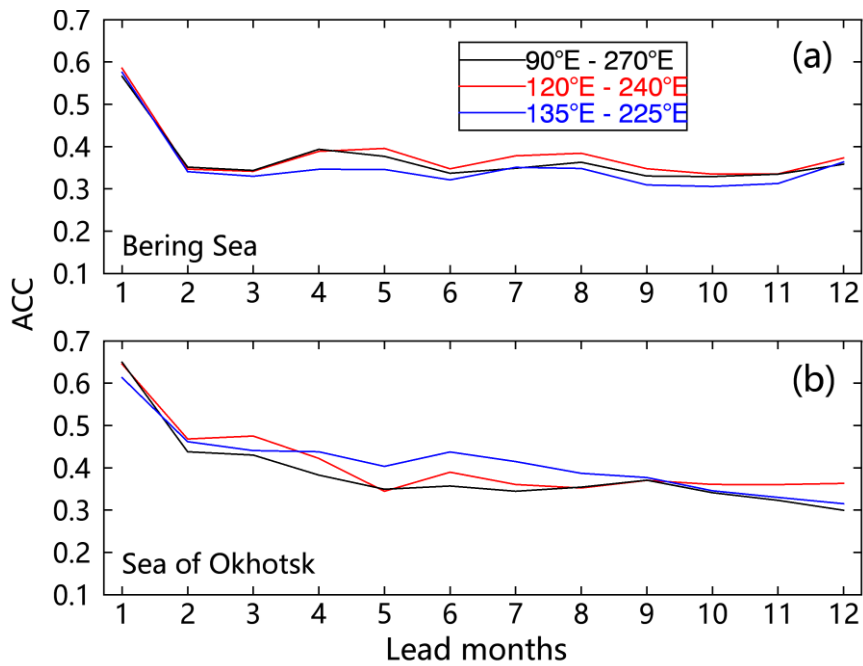
564

565 **Figure 11.** (a, b) Hindcast model skill (ACC) for detrended regional SIE forecasts  
 566 from 1982 to 2020 for the regional Markov model. (c, d) Same as (a, b) except for the  
 567 GFDL seasonal prediction system. (e, f) is the skill difference between these two  
 568 models. The black dots in (a-d) represent ACCs that are significantly above the 95%  
 569 confidence level, and the circles in (a-d) indicate months in which the model's skill  
 570 exceeds that of a persistence forecast. The black dots in (e-f) represent ACC  
 571 differences that are significant above the 95% confidence level.

572 Notably, the skill from the regional Markov model is higher than that from the  
573 GFDL seasonal prediction system during February to June at 3- to 6-month leads in  
574 the Bering Sea and during December to June at 1- to 8-month leads in the Sea of  
575 Okhotsk. In other words, the regional Markov model performs better in spring  
576 prediction using winter observations for the Bering Sea and autumn observations for  
577 the Sea of Okhotsk. Nevertheless, the regional Markov model slightly underperforms  
578 the GFDL seasonal prediction system in predictions during November to December  
579 using the previous winter and spring observations for the Bering Sea and using the  
580 previous winter observations for the Sea of Okhotsk. Overall, the regional Markov  
581 model delivers skillful SIE predictions in seasonal ice zones of the Pacific sector up to  
582 7 month lead times, an improvement from the 3 month leads displayed in the GFDL  
583 seasonal prediction system.

#### 584 **4.3 Sensitivity of model domain on the prediction skill**

585 We conducted a sensitivity analysis of the model domain on prediction skills in  
586 the Bering Sea and the Sea of Okhotsk with the same model configuration and  
587 different sizes of the model domain. The model domain is defined by 90°E to 270°E,  
588 120°E to 240°E and 135°E to 225°E respectively. The results show that the prediction  
589 skill patterns based on three model domains show high similarity in the Bering Sea  
590 and the skill based on the model domain (120°E to 240°E) is highest at all month  
591 leads. The prediction skill in the Sea of Okhotsk based on the model domain (135°E  
592 to 225°E) is highlighted at 5- to 8-month leads, but not well at 11- to 12-month leads.  
593 Although the models with different sizes of model domain have different prediction  
594 skills in the Bering Sea and the Sea of Okhotsk, the differences are not significant  
595 because all those model domains contain highly similar signals of climate variability.  
596 Therefore, the regional model is not highly sensitive to the size of the model domain  
597 within the Pacific-Arctic sector.



598

599 **Figure 12.** Cross-validated model skills of the regional Markov model with the  
600 same model configuration and different sizes of the model domain. (a) The skills are  
601 measured by the ACC between predictions and observations with trends from 1980 to  
602 2020 as a function of lead months in the Bering Sea. (b) is the same as (a) except for  
603 the Sea of Okhotsk. The model is configured by V9M16 in winter, V11M20 in spring,  
604 V5M10 in summer, and V5M7 in autumn. The ACC values are averaged over the area  
605 marked in the black box in Figure 1.

## 606 5 Conclusions

607 Here, we developed a regional Markov model to predict SIC in the Pacific-Arctic  
608 sector at the seasonal time scale. The model was constructed in the MEOF space so  
609 that the model can capture the covariability of the North Pacific climate system  
610 defined by 9 variables (SIC, OHC, SIT, SST, SAT, surface net radiative flux, surface  
611 net turbulent heat flux, and geopotential height and winds at 850 hPa). Based on  
612 cross-validation experiments, we selected model variables and mode truncations that  
613 provided the best results in each season. These model configurations were V9M16 for  
614 winter, V11M20 for spring, V5M10 for summer, and V5M7 for autumn.

615 The SIC prediction skill was evaluated at each grid cell and for all seasons using  
616 ACC. The regional Markov model's skill is superior to the skill derived from anomaly  
617 persistence, revealing the model's ability to capture more predictable SIC internal  
618 variability than anomaly persistence. The winter skill is about 0.4 in the Sea of  
619 Okhotsk and 0.5 in the northern Bering Sea at up to 12-month leads. The spring  
620 prediction shows a similar pattern but with a 0.1 increase in the ACC skill. The model  
621 skill in summer and autumn is more than 0.6 within the Arctic basin. Compared with  
622 the pan-Arctic seasonal prediction model, the regional Markov model distinctly  
623 improves the SIC prediction skill in the peripheral seas of the Pacific-Arctic sector.  
624 The regional model significantly enhances the correlation skill from the pan-Arctic  
625 model for 4- to 12-month lead predictions in the Bering Sea and 1- to 7-month lead  
626 predictions in the Sea of Okhotsk. The improvement is a 32% ACC increase in the  
627 Bering Sea and 18% in the Sea of Okhotsk. In addition, similar to the pan-Arctic  
628 Markov model, the regional model is not sensitive to the number of MEOF modes  
629 retained, which indicates that the performance of this Markov model is robust.

630 The model retains prediction skill after sea ice trend is removed or not. However,  
631 the detrended skill is notably lower, consistent with earlier sea ice prediction studies.  
632 When sea ice time series includes the trend, the model can skillfully predict SIE from  
633 January to November. The skill is particularly high for the predictions of summer and  
634 autumn sea ice at longer lead times, especially in July to November when the skill  
635 is  $>0.6$  even at a 12-month lead. Conversely, in May, the model skill is relatively low,  
636 especially at 4-8 lead months. Trend removal from predictions and observations  
637 results in a 53% reduction of the mean ACC for the entire Pacific-Arctic sector.  
638 However, the model only reduces 13% of the mean ACC from January to November  
639 at 1-2 lead months after the trend removal in the Bering Sea and the Sea of Okhotsk.  
640 This detrended analysis shows the model's capability of capturing sea ice internal  
641 variability beyond linear trends. Furthermore, the regional Markov model improves  
642 the detrended SIE prediction skill in the Pacific-Arctic sector to 7 month lead times  
643 from the 3 month lead skill displayed in the GFDL-FLOR seasonal prediction system.

644 The following reasons contribute to the improvements. First, the dominant climate  
645 variability in the northern mid-high latitudes mostly occurs in the Atlantic sector of  
646 the Arctic and subarctic, which dictates the leading MEOF mode in the pan-Arctic  
647 model. The unique characteristics of atmosphere-ocean-sea ice coupled relationships  
648 in the Pacific sector may not be included in the leading MEOF decompositions of the  
649 pan-Arctic climate system and thus are not correctly represented in the model. The  
650 regional model focuses on the Pacific-Arctic coupled atmosphere-ocean-sea ice  
651 system and captures the dominant regional climate variability. Second, the Pacific  
652 sector of the Arctic needs a different set of variables to maximize the model's  
653 predictability. We added OHC and SIT in the regional model, which provides a  
654 crucial source of predictability in winter and summer months respectively. We also  
655 include 850 hPa GPH and winds to represent dynamic atmospheric processes in  
656 winter and include turbulent heat flux to improve the model skill in spring. Finally,  
657 we constructed a superior model for each season, isolating the seasonally dominant  
658 processes separately.

659 It was also found that more modes were needed in the cold season to capture the  
660 predictable signal of SIC. This suggests that sea ice in cold seasons has more  
661 variability patterns compared with that in warm seasons, which may bring more errors  
662 in prediction. SIC trends are strongest in the warm season months, which may  
663 contribute to the smaller number of modes required. In addition to the climate system  
664 in the Arctic Basin, the coupled atmosphere-ocean-sea ice variability in the North  
665 Pacific plays a more important role in the cold season and needs more modes to  
666 capture the covariability signals.

667

668 *Data availability.* The sea ice concentration data were obtained from the National  
669 Snow and Ice Data Center (NSIDC, <https://nsidc.org/data/NSIDC-0079>, last access: 1  
670 July 2021, Comiso, 2017). Monthly SIT from the Pan-Arctic Ice-Ocean and  
671 Assimilating System (PIOMAS) can be obtained from the Polar Science Center (PSC)  
672 (<http://psc.apl.uw.edu/research/projects/arctic-sea-ice-volume->



673 [anomaly/data/model\\_grid](#), last access: 1 July 2021, Zhang and Rothrock, 2003). The  
674 ocean heat content in the upper 300 m, sea surface temperature, surface air  
675 temperature, surface net radiative flux, surface net turbulent heat flux, 850 hPa  
676 geopotential height, and 850 hPa wind vector from ERA5 can be obtained from the  
677 ECMWF (<https://cds.climate.copernicus.eu/cdsapp#!/search?type=dataset>, last access:  
678 1 July 2021, Hersbach et al., 2020).

679

680 *Supplement.* The supplement related to this article is available online at: **xxxx**.

681

682 *Author contributions.* YW, XY and HB conceived the idea for the protocol and  
683 experimental design. MB and HH provided primary support and guidance on the  
684 research. YW, YL and CL performed data processing. All authors drafted the  
685 manuscript, and contributed to manuscript revision.

686

687 *Competing interests.* The authors declare that they have no conflict of interest.

688

689 *Acknowledgements.* This work is supported by the Lamont endowment, the National  
690 Natural Science Foundation of China (42106223), and the China Postdoctoral Science  
691 Foundation (2020TQ0322). We thank the NSIDC for providing the sea ice  
692 concentration data on their website (<https://nsidc.org/data/NSIDC-0079>). Monthly  
693 SIT from the Pan-Arctic Ice-Ocean and Assimilating System (PIOMAS) can be  
694 obtained from the Polar Science Center (PSC)  
695 ([http://psc.apl.uw.edu/research/projects/arctic-sea-ice-volume-](http://psc.apl.uw.edu/research/projects/arctic-sea-ice-volume-anomaly/data/model_grid)  
696 [anomaly/data/model\\_grid](#)). The ocean heat content in the upper 300 m, sea surface  
697 temperature, surface air temperature, surface net radiative flux, surface net turbulent  
698 heat flux, 850 hPa geopotential height, and 850 hPa wind vector from ERA5 can be  
699 obtained from the ECMWF  
700 (<https://cds.climate.copernicus.eu/cdsapp#!/search?type=dataset>).

701

702 *Financial support.* This work is supported by the Lamont endowment, the National  
703 Natural Science Foundation of China (42106223; 42076185), the Natural Science  
704 Foundation of Shandong Province, China (ZR2021QD059), the China Postdoctoral  
705 Science Foundation (2020TQ0322), and the Open Funds for the Key Laboratory of  
706 Marine Geology and Environment, Institute of Oceanology, Chinese Academy of  
707 Sciences (MGE2021KG15; MGE2020KG04).

708 Lamont contribution number xxxx.

## 709 **References**

710

- 711 Andersson, T. R., Hosking, J. S., Perez-Ortiz, M., Paige, B., Elliott, A., Russell, C., Law, S., Jones, D.  
712 C., Wilkinson, J., Phillips, T., Byrne, J., Tietsche, S., Sarojini, B. B., Blanchard-  
713 Wrigglesworth, E., Aksenov, Y., Downie, R., and Shuckburgh, E.: Seasonal Arctic sea ice  
714 forecasting with probabilistic deep learning, *Nature Communications*, 12,  
715 <https://doi.org/10.1038/s41467-021-25257-4>, 2021.
- 716 Barnston, A. G. and Ropelewski, C. F.: Prediction of ENSO Episodes Using Canonical Correlation  
717 Analysis, *J. Clim.*, 5, 1316-1345, [https://doi.org/10.1175/1520-0442\(1992\)005<1316:poeuec>2.0.co;2](https://doi.org/10.1175/1520-0442(1992)005<1316:poeuec>2.0.co;2), 1992.
- 719 Blanchard-Wrigglesworth, E., Armour, K. C., Bitz, C. M., and DeWeaver, E.: Persistence and Inherent  
720 Predictability of Arctic Sea Ice in a GCM Ensemble and Observations, *J. Clim.*, 24, 231-250,  
721 <https://doi.org/10.1175/2010jcli3775.1>, 2011.
- 722 Blanchard-Wrigglesworth, E., Cullather, R., Wang, W., Zhang, J., and Bitz, C.: Model forecast skill  
723 and sensitivity to initial conditions in the seasonal Sea Ice Outlook, *Geophys. Res. Lett.*, 42,  
724 8042-8048, <https://doi.org/10.1002/2015GL065860>, 2015.
- 725 Blockley, E. W. and Peterson, K. A.: Improving Met Office seasonal predictions of Arctic sea ice using  
726 assimilation of CryoSat-2 thickness, *Cryosphere*, 12, 3419-3438, <https://doi.org/10.5194/tc-12-3419-2018>, 2018.
- 728 Bushuk, M. and Giannakis, D.: The Seasonality and Interannual Variability of Arctic Sea Ice  
729 Reemergence, *J. Clim.*, 30, 4657-4676, <https://doi.org/10.1175/jcli-d-16-0549.1>, 2017.
- 730 Bushuk, M., Msadek, R., Winton, M., Vecchi, G., Yang, X., Rosati, A., and Gudgel, R.: Regional  
731 Arctic sea-ice prediction: potential versus operational seasonal forecast skill, *CIDy*, 52, 2721-  
732 2743, <https://doi.org/10.1007/s00382-018-4288-y>, 2019.
- 733 Bushuk, M., Msadek, R., Winton, M., Vecchi, G. A., Gudgel, R., Rosati, A., and Yang, X.: Skillful  
734 regional prediction of Arctic sea ice on seasonal timescales, *Geophys. Res. Lett.*, 44, 4953-  
735 4964, <https://doi.org/10.1002/2017GL073155>, 2017a.
- 736 Bushuk, M., Msadek, R., Winton, M., Vecchi, G. A., Gudgel, R., Rosati, A., and Yang, X.: Summer  
737 Enhancement of Arctic Sea Ice Volume Anomalies in the September-Ice Zone, *J. Clim.*, 30,  
738 2341-2362, <https://doi.org/10.1175/jcli-d-16-0470.1>, 2017b.
- 739 Bushuk, M., Winton, M., Bonan, D. B., Blanchard-Wrigglesworth, E., and Delworth, T. L.: A  
740 Mechanism for the Arctic Sea Ice Spring Predictability Barrier, *Geophys. Res. Lett.*, 47,  
741 <https://doi.org/10.1029/2020gl088335>, 2020.

742 Bushuk, M., Winton, M., Haumann, F. A., Delworth, T., Lu, F., Zhang, Y., Jia, L., Zhang, L., Cooke,  
743 W., Harrison, M., Hurlin, B., Johnson, N. C., Kapnick, S. B., McHugh, C., Murakami, H.,  
744 Rosati, A., Tseng, K.-C., Wittenberg, A. T., Yang, X., and Zeng, F.: Seasonal Prediction and  
745 Predictability of Regional Antarctic Sea Ice, *J. Clim.*, 34, 6207-6233,  
746 <https://doi.org/10.1175/jcli-d-20-0965.1>, 2021.

747 Cañizares, R., Kaplan, A., Cane, M. A., Chen, D., and Zebiak, S. E.: Use of data assimilation via linear  
748 low-order models for the initialization of El Niño-Southern Oscillation predictions, *Journal of*  
749 *Geophysical Research: Oceans*, 106, 30947-30959, <https://doi.org/10.1029/2000JC000622>,  
750 2001.

751 Chen, D. and Yuan, X.: A Markov model for seasonal forecast of Antarctic sea ice, *J. Clim.*, 17, 3156-  
752 3168, [https://doi.org/10.1175/1520-0442\(2004\)017<3156:AMMFSF>2.0.CO;2](https://doi.org/10.1175/1520-0442(2004)017<3156:AMMFSF>2.0.CO;2), 2004.

753 Chen, T. C.: The structure and maintenance of stationary waves in the winter Northern Hemisphere,  
754 *Journal of the Atmospheric Sciences*, 62, 3637-3660, <https://doi.org/10.1175/jas3566.1>, 2005.

755 Cheng, W., Blanchard-Wrigglesworth, E., Bitz, C. M., Ladd, C., and Stabeno, P. J.: Diagnostic sea ice  
756 predictability in the pan-Arctic and US Arctic regional seas, *Geophys. Res. Lett.*, 43, 11688-  
757 11696, <https://doi.org/10.1002/2016gl070735>, 2016.

758 Chi, J. and Kim, H.-c.: Prediction of Arctic Sea Ice Concentration Using a Fully Data Driven Deep  
759 Neural Network, *Remote Sensing*, 9, <https://doi.org/10.3390/rs9121305>, 2017.

760 Cohen, J., Zhang, X., Francis, J., Jung, T., Kwok, R., Overland, J., Ballinger, T., Bhatt, U., Chen, H.,  
761 and Coumou, D.: Divergent consensus on Arctic amplification influence on midlatitude  
762 severe winter weather, *Nature Climate Change*, 10, 20-29, [https://doi.org/10.1038/s41558-](https://doi.org/10.1038/s41558-019-0662-y)  
763 019-0662-y, 2020.

764 Comiso, J. C.: Bootstrap Sea Ice Concentrations from Nimbus-7 SMMR and DMSP SSM/I-SSMIS,  
765 Version 3. NASA National Snow and Ice Data Center Distributed Active Archive Center,  
766 Boulder, Colorado USA, 2017.

767 Dai, P., Gao, Y., Counillon, F., Wang, Y., Kimmritz, M., and Langehaug, H. R.: Seasonal to decadal  
768 predictions of regional Arctic sea ice by assimilating sea surface temperature in the  
769 Norwegian Climate Prediction Model, *CIDy*, 54, 3863-3878, [https://doi.org/10.1007/s00382-](https://doi.org/10.1007/s00382-020-05196-4)  
770 020-05196-4, 2020.

771 Day, J. J., Hawkins, E., and Tietsche, S.: Will Arctic sea ice thickness initialization improve seasonal  
772 forecast skill?, *Geophys. Res. Lett.*, 41, 7566-7575, <https://doi.org/10.1002/2014gl061694>,  
773 2014a.

774 Day, J. J., Tietsche, S., and Hawkins, E.: Pan-Arctic and Regional Sea Ice Predictability: Initialization  
775 Month Dependence, *J. Clim.*, 27, 4371-4390, <https://doi.org/10.1175/JCLI-D-13-00614.1>,  
776 2014b.

777 Deser, C., Tomas, R., Alexander, M., and Lawrence, D.: The seasonal atmospheric response to  
778 projected Arctic sea ice loss in the late twenty-first century, *J. Clim.*, 23, 333-351,  
779 <https://doi.org/10.1175/2009JCLI3053.1>, 2010.

780 Francis, J. A. and Vavrus, S. J.: Evidence linking Arctic amplification to extreme weather in mid-  
781 latitudes, *Geophys. Res. Lett.*, 39, <https://doi.org/10.1029/2012GL051000>, 2012.

782 Frankignoul, C., Sennechael, N., and Cauchy, P.: Observed Atmospheric Response to Cold Season Sea  
783 Ice Variability in the Arctic, *J. Clim.*, 27, 1243-1254, [https://doi.org/10.1175/jcli-d-13-](https://doi.org/10.1175/jcli-d-13-00189.1)  
784 00189.1, 2014.

785 Gregory, W., Tsamados, M., Stroeve, J., and Sollich, P.: Regional September Sea Ice Forecasting with  
 786 Complex Networks and Gaussian Processes, *Weather and Forecasting*, 35, 793-806,  
 787 <https://doi.org/10.1175/WAF-D-19-0107.1>, 2020.

788 Guemas, V., Blanchard-Wrigglesworth, E., Chevallier, M., Day, J. J., Déqué, M., Doblus-Reyes, F. J.,  
 789 Fučkar, N. S., Germe, A., Hawkins, E., and Keeley, S.: A review on Arctic sea-ice  
 790 predictability and prediction on seasonal to decadal time-scales, *QJRMS*, 142, 546-561,  
 791 <https://doi.org/10.1002/qj.2401>, 2016a.

792 Guemas, V., Chevallier, M., Deque, M., Bellprat, O., and Doblus-Reyes, F.: Impact of sea ice  
 793 initialization on sea ice and atmosphere prediction skill on seasonal timescales, *Geophys. Res.*  
 794 *Lett.*, 43, 3889-3896, <https://doi.org/10.1002/2015gl066626>, 2016b.

795 Hamilton, L. C. and Stroeve, J.: 400 predictions: The search sea ice outlook 2008–2015, *Polar Geogr.*,  
 796 39, 274-287, <https://doi.org/10.1080/1088937X.2016.1234518>, 2016.

797 Hersbach, H., Bell, B., Berrisford, P., Hirahara, S., Horányi, A., Muñoz-Sabater, J., Nicolas, J.,  
 798 Peubey, C., Radu, R., and Schepers, D.: The ERA5 global reanalysis, *QJRMS*, 146, 1999-  
 799 2049, <https://doi.org/10.1002/qj.3803>, 2020.

800 Horvath, S., Stroeve, J., and Rajagopalan, B.: A linear mixed effects model for seasonal forecasts of  
 801 Arctic sea ice retreat, *Polar Geogr.*, doi: 10.1080/1088937X.2021.1987999, 2021. 1-18,  
 802 <https://doi.org/10.1080/1088937X.2021.1987999>, 2021.

803 Horvath, S., Stroeve, J., Rajagopalan, B., and Kleiber, W.: A Bayesian Logistic Regression for  
 804 Probabilistic Forecasts of the Minimum September Arctic Sea Ice Cover, *Earth and Space*  
 805 *Science*, 7, <https://doi.org/10.1029/2020ea001176>, 2020.

806 Huang, Y., Dong, X., Xi, B., Dolinar, E. K., and Stanfield, R. E.: Quantifying the Uncertainties of  
 807 Reanalyzed Arctic Cloud and Radiation Properties using Satellite-surface Observations, *CIDy*,  
 808 30, 8007-8029, <https://doi.org/10.1175/JCLI-D-16-0722.1>, 2015.

809 Kapsch, M. L., Graverson, R. G., and Tjernström, M.: Springtime atmospheric energy transport and the  
 810 control of Arctic summer sea-ice extent, *Nature Climate Change*, 3, 744-748,  
 811 <https://doi.org/10.1038/nclimate1884>, 2013.

812 Kim, K.-Y., Hamlington, B. D., Na, H., and Kim, J.: Mechanism of seasonal Arctic sea ice evolution  
 813 and Arctic amplification, *The Cryosphere*, 10, 2191-2202, [https://doi.org/10.5194/tc-10-2191-](https://doi.org/10.5194/tc-10-2191-2016)  
 814 2016, 2016.

815 Kimmritz, M., Counillon, F., Smedsrud, L. H., Bethke, I., Keenlyside, N., Ogawa, F., and Wang, Y.:  
 816 Impact of Ocean and Sea Ice Initialisation On Seasonal Prediction Skill in the Arctic, *Journal*  
 817 *of Advances in Modeling Earth Systems*, 11, 4147-4166,  
 818 <https://doi.org/10.1029/2019ms001825>, 2019.

819 Koenigk, T., Caian, M., Nikulin, G., and Schimanke, S.: Regional Arctic sea ice variations as predictor  
 820 for winter climate conditions, *CIDy*, 46, 317-337, <https://doi.org/10.1007/s00382-015-2586-1>,  
 821 2016.

822 Lee, S., Gong, T., Feldstein, S. B., Screen, J. A., and Simmonds, I.: Revisiting the Cause of the 1989–  
 823 2009 Arctic Surface Warming Using the Surface Energy Budget: Downward Infrared  
 824 Radiation Dominates the Surface Fluxes, *Geophys. Res. Lett.*, 44, 10654-10661,  
 825 <https://doi.org/10.1002/2017GL075375>, 2017.

826 Lenetsky, J. E., Tremblay, B., Brunette, C., and Meneghello, G.: Subseasonal Predictability of Arctic  
 827 Ocean Sea Ice Conditions: Bering Strait and Ekman-Driven Ocean Heat Transport, *J. Clim.*,  
 828 34, 4449-4462, <https://doi.org/10.1175/jcli-d-20-0544.1>, 2021.

829 Lindsay, R., Zhang, J., Schweiger, A., and Steele, M.: Seasonal predictions of ice extent in the Arctic  
830 Ocean, *Journal of Geophysical Research: Oceans*, 113,  
831 <https://doi.org/10.1029/2007JC004259>, 2008.

832 Liu, Y. and Key, J. R.: Less winter cloud aids summer 2013 Arctic sea ice return from 2012 minimum,  
833 *Environmental Research Letters*, 9, 044002, <https://doi.org/10.1088/1748-9326/9/4/044002>,  
834 2014.

835 Luo, B., Luo, D., Wu, L., Zhong, L., and Simmonds, I.: Atmospheric circulation patterns which  
836 promote winter Arctic sea ice decline, *Environmental Research Letters*, 12, 1-13,  
837 <https://doi.org/10.1088/1748-9326/aa69d0>, 2017.

838 Meleshko, V., Kattsov, V., Mirvis, V., Baidin, A., Pavlova, T., and Govorkova, V.: Is there a link  
839 between Arctic sea ice loss and increasing frequency of extremely cold winters in Eurasia and  
840 North America? Synthesis of current research, *Russian Meteorology and Hydrology*, 43, 743-  
841 755, <https://doi.org/10.3103/S1068373918110055>, 2018.

842 Morioka, Y., Iovino, D., Cipollone, A., Masina, S., and Behera, S.: Summertime sea-ice prediction in  
843 the Weddell Sea improved by sea-ice thickness initialization, *Sci. Rep.*, 11,  
844 <https://doi.org/10.1038/s41598-021-91042-4>, 2021.

845 Msadek, R., Vecchi, G. A., Winton, M., and Gudgel, R. G.: Importance of initial conditions in seasonal  
846 predictions of Arctic sea ice extent, *Geophys. Res. Lett.*, 41, 5208-5215,  
847 <https://doi.org/10.1002/2014gl060799>, 2014.

848 Peterson, A. K., Fer, I., McPhee, M. G., and Randelhoff, A.: Turbulent heat and momentum fluxes in  
849 the upper ocean under Arctic sea ice, *Journal of Geophysical Research: Oceans*, 122, 1439-  
850 1456, <https://doi.org/10.1002/2016JC012283>, 2017.

851 Peterson, K. A., Arribas, A., Hewitt, H., Keen, A., Lea, D., and McLaren, A.: Assessing the forecast  
852 skill of Arctic sea ice extent in the GloSea4 seasonal prediction system, *CIJy*, 44, 147-162,  
853 <https://doi.org/10.1007/s00382-014-2190-9>, 2015.

854 Petty, A., Schröder, D., Stroeve, J., Markus, T., Miller, J., Kurtz, N., Feltham, D., and Flocco, D.:  
855 Skillful spring forecasts of September Arctic sea ice extent using passive microwave sea ice  
856 observations, *Earth's Future*, 5, 254-263, <https://doi.org/10.1002/2016EF000495>, 2017.

857 Porter, D. F., Cassano, J. J., and Serreze, M. C.: Analysis of the Arctic atmospheric energy budget in  
858 WRF: A comparison with reanalyses and satellite observations, *Journal of Geophysical  
859 Research Atmospheres*, 116, <https://doi.org/10.1029/2011JD016622>, 2011.

860 Sévellec, F., Fedorov, A. V., and Liu, W.: Arctic sea-ice decline weakens the Atlantic meridional  
861 overturning circulation, *Nature Climate Change*, 7, 604-610,  
862 <https://doi.org/10.1038/NCLIMATE3353>, 2017.

863 Schweiger, A., Lindsay, R., Zhang, J., Steele, M., Stern, H., and Kwok, R.: Uncertainty in modeled  
864 Arctic sea ice volume, *Journal of Geophysical Research-Oceans*, 116,  
865 <https://doi.org/10.1029/2011jc007084>, 2011.

866 Screen, J. A. and Francis, J. A.: Contribution of sea-ice loss to Arctic amplification is regulated by  
867 Pacific Ocean decadal variability, *Nature Climate Change*, 6, 856-860,  
868 <https://doi.org/10.1038/NCLIMATE3011>, 2016.

869 Screen, J. A., Simmonds, I., Deser, C., and Tomas, R.: The atmospheric response to three decades of  
870 observed Arctic sea ice loss, *J. Clim.*, 26, 1230-1248, <https://doi.org/10.1175/JCLI-D-12-00063.1>, 2013.

871

872 Sigmond, M., Fyfe, J. C., Flato, G. M., Kharin, V. V., and Merryfield, W. J.: Seasonal forecast skill of  
873 Arctic sea ice area in a dynamical forecast system, *Geophys. Res. Lett.*, 40, 529-534,  
874 <https://doi.org/10.1002/grl.50129>, 2013.

875 Smith, D. M., Dunstone, N. J., Scaife, A. A., Fiedler, E. K., Copesey, D., and Hardiman, S. C.:  
876 Atmospheric response to Arctic and Antarctic sea ice: The importance of ocean–atmosphere  
877 coupling and the background state, *J. Clim.*, 30, 4547-4565, <https://doi.org/10.1175/JCLI-D-18-0100.1>, 2017.

879 Smith, L. C. and Stephenson, S. R.: New Trans-Arctic shipping routes navigable by midcentury,  
880 *Proceedings of the National Academy of Sciences*, 110, E1191-E1195,  
881 <https://doi.org/10.1073/pnas.1214212110>, 2013.

882 Swart, N.: Natural causes of Arctic sea-ice loss, *Nature Climate Change*, 7, 239-241,  
883 <https://doi.org/10.1038/nclimate3254>, 2017.

884 Tian, T., Yang, S., Karami, M. P., Massonnet, F., Kruschke, T., and Koenigk, T.: Benefits of sea ice  
885 initialization for the interannual-to-decadal climate prediction skill in the Arctic in EC-Earth3,  
886 *Geoscientific Model Development*, 14, 4283-4305, <https://doi.org/10.5194/gmd-14-4283-2021>, 2021.

888 Ting, M. F.: MAINTENANCE OF NORTHERN SUMMER STATIONARY WAVES IN A GCM,  
889 *Journal of the Atmospheric Sciences*, 51, 3286-3308, [https://doi.org/10.1175/1520-0469\(1994\)051<3286:monssw>2.0.co;2](https://doi.org/10.1175/1520-0469(1994)051<3286:monssw>2.0.co;2), 1994.

891 Wang, L., Scott, K. A., and Clausi, D. A.: Sea ice concentration estimation during freeze-up from SAR  
892 imagery using a convolutional neural network, *Remote Sensing*, 9, 408,  
893 <https://doi.org/10.3390/rs9050408>, 2017.

894 Wang, L., Yuan, X., and Li, C.: Subseasonal forecast of Arctic sea ice concentration via statistical  
895 approaches, *CIDy*, 52, 4953-4971, <https://doi.org/10.1007/s00382-018-4426-6>, 2019a.

896 Wang, L., Yuan, X., Ting, M., and Li, C.: Predicting summer Arctic sea ice concentration intraseasonal  
897 variability using a vector autoregressive model, *J. Clim.*, 29, 1529-1543,  
898 <https://doi.org/10.1175/JCLI-D-15-0313.1>, 2016.

899 Wang, Y., Yuan, X., Bi, H., Liang, Y., Huang, H., Zhang, Z., and Liu, Y.: The Contributions of Winter  
900 Cloud Anomalies in 2011 to the Summer Sea-Ice Rebound in 2012 in the Antarctic, *Journal*  
901 *of Geophysical Research: Atmospheres*, 124, 3435-3447,  
902 <https://doi.org/10.1029/2018JD029435>, 2019b.

903 Wu, B., Wang, J., and Walsh, J. E.: Dipole Anomaly in the Winter Arctic Atmosphere and Its  
904 Association with Sea Ice Motion, *J. Clim.*, 19, 210-225, <https://doi.org/10.1175/JCLI3619.1>,  
905 2006.

906 Wu, Q., Cheng, L., Chan, D., Yao, Y., Hu, H., and Yao, Y.: Suppressed midlatitude summer  
907 atmospheric warming by Arctic sea ice loss during 1979–2012, *Geophys. Res. Lett.*, 43, 2792-  
908 2800, <https://doi.org/10.1002/2016GL068059>, 2016.

909 Wu, Q., Yan, Y., and Chen, D.: A linear Markov model for East Asian monsoon seasonal forecast, *J.*  
910 *Clim.*, 26, 5183-5195, <https://doi.org/10.1175/JCLI-D-12-00408.1>, 2013.

911 Xie, J., Counillon, F., Bertino, L., Tian-Kunze, X., and Kaleschke, L.: Benefits of assimilating thin sea  
912 ice thickness from SMOS into the TOPAZ system, *Cryosphere*, 10, 2745-2761,  
913 <https://doi.org/10.5194/tc-10-2745-2016>, 2016.

914 Xue, Y., Leetmaa, A., and Ji, M.: ENSO prediction with Markov models: The impact of sea level, *J.*  
915 *Clim.*, 13, 849-871, [https://doi.org/10.1175/1520-0442\(2000\)013,2000](https://doi.org/10.1175/1520-0442(2000)013,2000).

916 Yuan, X., Chen, D., Li, C., Wang, L., and Wang, W.: Arctic sea ice seasonal prediction by a linear  
917 Markov model, *J. Clim.*, 29, 8151-8173, <https://doi.org/10.1175/JCLI-D-15-0858.1>, 2016.  
918 Zhang, J. L. and Rothrock, D. A.: Modeling global sea ice with a thickness and enthalpy distribution  
919 model in generalized curvilinear coordinates, *MWRv*, 131, 845-861,  
920 [https://doi.org/10.1175/1520-0493\(2003\)131<0845:mgsiwa>2.0.co;2](https://doi.org/10.1175/1520-0493(2003)131<0845:mgsiwa>2.0.co;2), 2003.  
921 Zuo, H., Balmaseda, M. A., Tietsche, S., Mogensen, K., and Mayer, M.: The ECMWF operational  
922 ensemble reanalysis-analysis system for ocean and sea ice: a description of the system and  
923 assessment, *Ocean Sci.*, 15, 779-808, <https://doi.org/10.5194/os-15-779-2019>, 2019.  
924